BELLCOMM, INC.
955 L'ENFANT PLAZA NORTH, S.W. WASHINGTON, D.C. 20024

COVER SHEET FOR TECHNICAL MEMORANDUM

TITLE- Reduction in Lunar Surface Visibility Due to Glare During a Landing into the Sun

TM- 68-2013-5

DATE- September 30, 1968

FILING CASE NO(S)- 310

AUTHOR(S)- R. Troester

FILING SUBJECT(S)- (ASSIGNED BY AUTHOR(S)- Lunar Landing Visibility, Glare, RCS Contamination

ABSTRACT

A major obstacle to the consideration of a lunar landing against the sun, such as a descent in the lunar afternoon or posigrade approaches in the lunar morning, has been the uncertainty in the effect of glare on the visibility of lunar surface obstacles. An analytical glare model is used in this paper to investigate the decrease in scene contrast brought about by the two main contributors to glare: direct solar dazzle in the astronaut's eyes and light scattered by any LM RCS exhaust residue on the forward window. Dazzle is computed with the aid of an empirical equation representing the average results of several experimental studies. The scatter model is based on diffraction and geometrical optics and is fitted to scatter measurements made of the LM RCS residue at MSC in 1966. On the basis of these measurements the lower bound for the fraction of the window surface covered by scattering particles, σ, is found to be about 0.5%. The upper bound for contamination during the lunar landing is not known but is unlikely to be more than 10%.

It is conservatively assumed that the visibility of 0.5 degree wide obstacles near the landing point will be acceptable when the contrast with glare of a 10° slope is 0.07 or above. With this criterion, contrast levels are unacceptable for low forward sun elevations (less than 20°), even if the eye is shielded from the sun, except for low values of σ. At sun elevations of 20° to 60° contrast levels without dazzle are quite good for σ less than 1.5% (three times the MSC measurement). At high forward sun elevations (40° to 60°) contrast levels remain acceptable for σ as high as 10% if the astronaut's eyes are shielded from the sun. For all elevations, an approach azimuth to the right of 180° (as seen by the astronauts) does not improve contrast significantly, but employment of an azimuth 20° to 30° to the left results in excellent

SEE REVERSE SIDE FOR DISTRIBUTION LIST

DISTRIBUTION

COMPLETE MEMORANDUM TO

CORRESPONDENCE FILES:

OFFICIAL FILE COPY
plus one white copy for each additional case referenced

TECHNICAL LIBRARY (4)

NASA Headquarters

W. O. Armstrong/MTX
P. E. Culbertson/MLA
J. H. Disher/MLD
S. Dowrnik/SL
J. Edberg/SL
E. W. Hall/MTG
T. A. Keegan/MA-2
R. S. Kraemer/SL
D. R. Lord/MTD
B. G. Noblitt/MTY
A. D. Schnyer/MTV
M. G. Waugh/MTP
J. W. Wild/MTE

Manned Spacecraft Center

C. Covington/ET23
D. E. Fielder/HA
J. Funk/FM8
W. N. Hess/TA
G. C. Miller/ET23
M. A. Silveira/ET
J. M. West/AE

Marshall Space Flight Center

H. S. Becker/R-AS-DIR
E. D. Geissler/R-AERO-DIR
R. J. Harris/R-AS-MP
F. L. Williams/R-AS-DIR

Kennedy Space Center

R. J. Cerrato/DE-FSO
J. P. Claybourne/DE-FSO
R. C. Hock/AA
N. P. Salvail/DE-FSO

Goddard Space Flight Center

J. E. Ainsworth/621

GSFC (Continued)

G. Hogan/733
W. C. Nyberg/733
L. Roach/733
N. W. Spencer/620

Ames Research Center

H. Hornby/MO
L. Roberts/M
A. Seiff/SV
K. F. Sinclair/MS
P. R. Swan/MS

JPL

R. G. Brereton/131
C. W. Cole/261
P. Eckman/130
J. Long/161
R. Mackin/325
R. Parks/20
R. R. Stephenson/311

Langley Research Center

W. R. Hook/60.300/156

Bellcomm

F. G. Allen
G. M. Anderson
C. Bidgood
A. P. Boysen, Jr.
G. A. Briggs
D. A. Chisholm
M. M. Cutler
C. L. Davis
D. A. DeGraaf
E. M. Grenning
D. A. Hagner
J. J. Hibbert
N. W. Hinners
B. T. Howard
D. B. James
J. Kranton
H. S. London
E. D. Marion
K. E. Martersteck
J. Z. Menard
G. T. Orrok
I. M. Ross
R. V. Sperry
J. W. Timko
W. B. Thompson

BA-146 (8-64)

ABSTRACT (contd.)

contrast due to blockage of sunlight by the LM structure. In this case and even in a descent directly into the sun (except for the very worst case values of σ) the range of sun angles providing good visibility is three to five times that available in the present landing at lunar dawn. This could provide launch opportunities to the same lunar landing site for as many as three successive days.

To minimize the amount of sunlight entering the LM, it is recommended that the LM Pilot's window be covered during a landing against the sun, if this is operationally feasible. Also, if a 20°-30° left azimuth cannot be employed, the upper portion of the Commander's window should be shaded down to the horizon, and in any landing approach the far left side of the Commander's window should be covered to block reflected glare from the LM RCS quad mounted outside.

CONTENTS

1.0 Introduction & Conclusions

1.1 Study Summary

1.2 Study Results and Recommendations

2.0 The Optical Environment During Descent

2.1 LM Structure Affecting Vision

2.2 Differences in Sun-Ahead and Sun-Behind Lighting

3.0 Analysis of Lunar Glare

3.1 Visibility and Contrast Under Glare Conditions

3.2 Dazzle

3.3 Scatter

3.1.1 Sources of Scatter Contaminants

3.3.2 The Scatter Model

3.3.2.1 Single Particle Scattering

3.3.2.2 Particle Size Distribution

3.3.2.3 Scatter Luminance

3.3.2.4 Film Effects

3.3.2.5 Scatter Characteristics

3.3.3 Fitting of the Scattering Model to the MSC Data

3.3.4 Scatter of Light Reflected from the Lunar Surface

4.0 The Glare Model

4.1 Characteristics

4.2 Errors

5.0 Comparison with Previous Studies

CONTENTS (contd.)

Appendix A List of Principal Symbols

B Derivation of the Total Scattered Intensity of a Size Distribution of Particles

C Negative Exponential Distribution: Scattered Intensity

D Uniform Distribution: Scattered Intensity

BELLCOMM, INC.
955 L'ENFANT PLAZA NORTH, S.W. WASHINGTON, D.C. 20024

SUBJECT: Reduction in Lunar Surface Visibility Due to Glare During a Landing into the Sun - Case 310

DATE: September 30, 1968

FROM: R. Troester

TM-68-2013-5

TECHNICAL MEMORANDUM

1.0 INTRODUCTION AND CONCLUSIONS

The present lunar mission design requires a landing at lunar dawn with the sun behind the LM and between 6 and 20 degrees above the horizon. The choice of this range of sun angles is the result of several studies of lunar lighting conditions, all of which show that a wash-out region exists for sun angles extending from roughly 4° below the line-of-sight to 20° or more above and some 10° to either side. In this region contrast differences between surface features are practically nil.

The studies also show that really excellent contrast is possible in any approach where the sun is again low in the sky but now in front of the LM instead of behind it. Such a situation would occur in a) a lunar afternoon landing, b) a "buttonhook" approach where the LM overshoots the landing site and retraces its path, or c) in a posigrade lunar orbit and approach at lunar dawn. In this paper, for conciseness, all such trajectories will be called "Sun Ahead" landings and abreviated SA, while the present approach will be referred to as a "Sun Behind" landing, abreviated SB.

The clarity of surface texture in a Sun Ahead landing would be even better than with the sun behind the LM, and surface details down range of the landing site would not be washed-out as they inevitably are with the present range of sun angles. The lunar surface would appear darker than in the SB approach, but would still be acceptably bright.

Insofar as these considerations are concerned an approach against the sun would be at least as advantageous as the present approach and its acceptance in the form of an afternoon landing would double the number of launch opportunities per month to a given site. There are several objections to an afternoon approach, among them such problems as the generally higher surface temperature and the time limit placed on lunar staytime by sunset. But a major factor has been the uncertainty in the visual effect of the glare from direct sunlight on the LM Commander's window and in his eyes.

1.1 Study Summary

Glare effects during the LM descent and the accompanying degradation of vision are the subject of this study. The word "glare" is a blanket designation for all extraneous light which is introduced into the line of sight, whether indirectly by reflection or scatter from external surfaces or directly by dazzle from a bright light in the field of view. Both types of glare are a very real problem as can be attested by anyone who has driven a car with a dirty windshield toward the setting or rising sun.

In order to provide a proper basis for the discussion of glare, Section 2 of this report is taken up with a general discussion of the differences in the lunar terrain lighting between SB and SA Landings and of the structure of the LM insofar as it affects the astronaut's vision. Some operational changes to eliminate potential sources of glare in the landing approach are discussed beiefly.

Section 3 begins with a calculation of the contrast under glare conditions and a definition of the relative contrast, or ratio of contrast with glare to contrast without glare, which is the principal contribution of this study. In Section 3.2 a survey of the experimental work on dazzle is carried out in order to select an empirical equation for dazzle in the glare model. Scatter glare from the commander's window is taken up in Section 3.3, beginning with a consideration of the possible sources of window contamination. The principal contaminant of those considered is residue from the LM RCS plume, and the known properties of this residue are reviewed. A theoretical model for the scatter is next developed, based on classical diffraction and geometrical optics. This model is fitted to data from a MSC residue deposition experiment in order to derive a realistic range of values for the principal parameters of the scattering model, primirily the scattering coefficient, σ, the fraction of the window covered by scatterers. The development of the scatter model is completed with the consideration of the amount of scatter due to light reflected from the lunar surface (a secondary source); this is found to be insignificant. In Section 4 the characteristics of the complete glare model are investigated and the error caused by the range in the scatter model parameters and the uncertainty in the dazzle formula is estimated. Finally, in Section 5 the results of this study are compared with the conclusions of several earlier studies which have some bearing on the LM glare problem.

1.2 Study Results and Recommendations

In a Sun Ahead landing lunar surface contrast, under certain conditions, meets or exceeds levels which have been

proposed to provide minimum acceptable visibility for a lunar landing (4.1).*

For the range of sun elevations from 20° to 60° above the forward horizon (the normal values for an afternoon landing) contrast is quite good, as good as for a sun angle 2° or 3° below the line of sight, if the astronaut's eye can be shielded from direct sunlight and if the scattering coefficient, σ, is less than 1.5%. If σ is as high as 10% or if the sun shines directly in the eye, scene contrast is still marginally acceptable for sun elevations near 40°. At higher sun elevations than 40° acceptably high contrasts are possible even if σ is as much as 10% but not if direct sunlight strikes the eye. At sun elevations less than 20°, scene contrast is too degraded by scatter glare to be acceptable, except for low values of σ, even if the eye is shielded from the sun (4.1).

At any sun elevation, an approach azimuth to the right of 180° (as seen by the astronauts) does not improve contrast significantly over that available at 180°; however, employment of an azimuth 20° to 30° to the left results in excellent contrast, especially at low sun angles, since the LM forward beam then blocks the sunlight from the Commander's window and eye (Figures 5 and 17). The range of sun angles providing good scene contrast is much wider in this type of landing than in a SB landing and, depending on σ, may still be as much as 3 to 5 times wider than in a SB landing, even if the sun is not blocked from the window. This wider band of sun angles could allow launch windows to a single landing site for as many as three successive days (4.1).

Five potential sources of glare which will affect the contrast levels have been isolated in this study. They are:

° Solar Dazzle

For those vehicle orientations which are such that the sun may shine directly in the astronaut's eye, solar dazzle generally is a more important source of glare than is scatter (4.1). However, even if no pre-mission provision were made against dazzle, the astronaut's automatic reaction would be to attempt to shield his eyes in some manner; thus it is unrealistic to reject a particular lunar landing approach solely because of the potential degradation of vision due to this source of glare (3.2). As an operational solution, it is recommended that the approach path be maintained 20° to 30°

*The numbers in parentheses refer to the section which amplifies the discussion or supports the conclusions given.

or more to the left (as seen by the astronauts) of the eye-sun line so that the LM structure will block the sunlight from the commander's eye. Furthermore, if it is considered feasible, the upper portion of the commander's window might be shaded down to the horizon, leaving the lower portion clear. This would enable an approach directly against the sun (2.1).

° Solar Scatter

The characteristics of scatter glare (sunlight scattered from any LM RCS exhaust residue on the commander's window) are dependent upon three parameters of the LM-RCS exhaust residue: the index of refraction, n_s, of the scattering particles in the residue; the mean diameter, d_{mean}, of the particles, and the fraction of the window area covered by scatterers, here called the scattering coefficient, σ (3.3.2). A fit of the scatter model to available experimental data indicates that n_s can be taken between 1.5 and 1.6. The mean diameter is indeterminate, but probably in the range of 3 to 100 microns. (Since the principal scattering mechanism over the range of angles of interest is refraction, which does not depend upon d_{mean}, this uncertainty in d_{mean} is not very serious.) The scattering coefficient is found to be about 0.5%. This should be thought of as a lower bound on σ; the upper bound for the lunar landing mission is not known but is perhaps as much as 10% . For such high values of σ, solar scatter is more serious than solar dazzle (3.3.3).

° Lunar Scatter

In all cases, lunar scatter, that is, light from the lunar surface scattered by the residue on the window, is negligible. The integrated illumination from the lunar surface on the commander's window, even at low gate, never exceeds 120 ft-cd, or 1% of the solar contribution, and the portion of this light scattered into the line of sight is too small to noticeably dimish the general scene contrast (3.3.4).

° Window Reflection

A potentially serious glare problem may arise from the light reflected by the antifog coating on the forward window if sunlight is allowed to enter the LM cabin and strike the window either directly through the overhead docking window (as could happen in the nominal approach)

or after reflection off the suit and cabin fittings. This glare source by itself could reduce the scene contrast by 80% or more (2.1). It is recommended that in any Sun Ahead landing that the LM Pilot's window be covered by its shade, if this is operationally feasible, to minimize the amount of sunlight which enters the LM cabin.

° RCS Quad Dazzle

Since the RCS quad on the Commander's side could reflect a distracting amount of light into his eyes over a wide range of vehicle orientations and sun elevations, it is recommended that the far left portion of the commander's window be covered to eliminate this dazzle source (2.1).

2.0 THE OPTICAL ENVIRONMENT DURING DESCENT

2.1 LM Structure Affecting Vision

During the descent from higate the LM pilot will be occupied in monitoring the LM Guidance Computer in calling out angle markings on the Landing Point Designator (LPD) reticle to the commander so that the commander, observing the terrain through the left forward window, can determine the current landing point and search for the presence of any obstacles which would require a redesignation.

The interior illumination the pilot will need to read his checklists and operate the Display and Keyboard (DSKY) is provided by a set of floodlights on each side of the cabin, consisting of a flood in each astronaut's overhead aimed toward the front panel and another one just under each forward window, both of which are dimable, and three fixed level lights recessed under each bank of the side panels (see Figure 1). A two-level portable utility light for each astronaut is supplied for use as needed. On the panels, the numeric read-outs, displays and panel legends are integrally lighted and are dimable, as are the caution and warning lights. The side panel lighting can be extinguished independently of the remaining lighting. A final source of internal illumination is provided by the toggle switch tips and LPD reticle which are faintly radioluminescent (≈ .05 ft.L).

The two LM astronauts will be helmeted and wearing the white beta cloth Integrated Thermal Meteoroid Garment (ITMG) during the descent. The helmet is a fishbowl made of Lexan polycarbonate plastic coated for antireflection on both surfaces. The results of the LM Simulator Lighting/Reflection Review at MSC in late October 1967 (Reference 39) indicate that reflections

from the cabin lights and surfaces on the helmet will not be noticeable. However, reflections due to any sunlight streaming through the LM windows may present a more serious problem, especially if the helmet becomes scratched.

The LM is equipped with three windows: two triangularly shaped windows some two feet square in area which are canted outward at the top in the forward bulkhead about a foot in front of the astronauts and a third 5x12 inch docking window in the commander's overhead. All three (Figure 2) are constructed of two panes of glass, the gap between vented to space, and are equipped with a snapable, nearly opaque shade which covers the windows during the lunar sleep period and during use of the Alignment Optical Telescope (AOT). In an against-the-sun descent, if it is operationally feasible, the shade should be drawn over the LM pilot's window to attempt to minimize the solar searchlight effect and reflections within the LM. It is obviously impossible to draw the shade entirely over the commander's window, but, as shown below, a redesignation of 20°-30° to the left during descent will have the same effect.

A Chemcor pressure glass forms the inner pane of the commander's window. Its inner surface is covered with a High Efficiency Antireflective (HEA) coating (Figure 2). The outer surface is coated with a resistive antifog coating and marked with the LPD reticle. An inch separates the inner pane from the outer, the inner surface of which is also marked with the LPD and coated with HEA. The outer surface of the outer pane has a Wide Band Hot Mirror (WBHM) coating which serves to screen both infrared and ultraviolet from the spacecraft.

The HEA coatings reduce transmission loss due to (normal) reflection off the surfaces on which they are applied from roughly 4% to only .5-1% over most of the visible spectrum. The transmission loss due to the WBHM coating is 5 to 10% (Reference 46) but is not objectionable, especially in the landing phase with its very high exterior illumination, where some filtering is even desirable.

The antifog coating could create a more serious problem. It consists of three monomolecular layers of stannous oxide, the first layer covering the entire triangular pane, the second extending about half-way from the top, and the third, one-third down, giving the window a yellow appearance at the top, which shades through straw to clear at the bottom. (This odd pattern is used to develop a uniform electrical resistance across the width of the pane.) In addition to reducing the total average window transmission to 76%, the thin metal coat also has the characteristics of a one way mirror. In other words, the LM windows will appear as opaque mirrors when the cabin lighting

reflected in the window is brighter than the exterior and will appear transparent if the LM cabin is darker than the exterior. In the present mission design, it is thought that the 11 inch glare screens between the center panels and windows (shown in Figure 1) and the use of low cabin illumination will prevent this characteristic from becoming a problem. It may also be possible to apply an anti-reflection coating over the antifog coating (Reference 46).

However, if direct sunlight is allowed to enter the cabin in a Sun-Ahead approach, the resulting reflection glare in the commander's window may be a serious bar to vision. The reflection of the sunlit ITMG in the window, for example, could easily appear 4 to 10 times brighter than the lunar surface which the astronaut is trying to observe through it. Such a reflected veil of light superimposed over the field of view would lower the effective lunar surface contrast by 4/5 or more. This drastic effect on visibility underscores the need to reduce window reflections to a minimum.

Looking out through his window, the commander can see a portion of the LM structure, i.e., RCS quad I which is located about 3-1/2 feet from the window, the left forward beam, and the lower part of the forward leg and landing pad. The precise amount visible depends on the location of the commander's eye which is nominally at the "design eye" position. The LM surface about the forward window is painted with black Pyromark silicone paint and neither it nor the landing gear present a significant glare problem. On the other hand the ribbed, gold-colored quad I RCS nozzles are a possible secondary glare source for a large range of sun angles and vehicle orientations. They are located far to the left (60°-80°) of the line of sight, but if the commander should chance to glance at them, his visual adaptation may be impaired for at least several seconds. Thus, some thought should be given to the means of blocking them out of his field of view, such as modifying the shade to cover the left-hand portion of the window.

The final obstacle in the commander's line of sight to the landing point is the descent engine plume, which, since the gas has an index of refraction somewhat different from 1, will act as a weakly refracting medium, distorting the terrain visible through it. The effect is expected to be small and will be evaluated during the first CSM/LM Operations Mission.

2.2 Differences in Sun-Ahead and Sun-Behind Lighting

The lunar surface that the commander sees, looking through his window, will appear somewhat different if the sun is ahead of the LM rather than behind. If the windows are oriented toward the lunar surface during the seven minute braking phase

from pericynthion to higate, then in a SB approach the astronauts will see a mostly sunlit hemisphere while in SA approach all but the final 20 or 30 degrees of latitude will be in relatively dark earthshine. At higate, 6 miles from the landing site, the LM, which was nearly horizontal, pitches up 50°, and the commander has his first view of the landing area through the left forward window. In the standard trajectory (Reference 26) the LM continues its descent from higate to logate - the visibility phase - at a nearly constant flight path angle of 15°-17° and pitches slowly from 40° back from the vertical at higate to about 20° at logate. These trajectory angles will be employed in this report for both SB and SA landings, except in some figures where the flight path angle (also called the look angle) is taken as 14.4° and the pitch angle as 43° for comparison with an earlier glare analysis.

The optimum sun angle* for a SB landing is about 7°, but for a SA (lunar afternoon) landing the sun elevation* from the horizon would be higher, a minimum of about 22°, to ensure daylight during the full 44 hr. contingency staytime on the lunar surface. To permit a one day launch window a variation in sun angle of about 13° must be allowed for; hence, the range of sun elevations of maximum interest in a SA landing is about 22° to 35° above the forward horizon. Higher sun elevations may also be of interest in later missions and low sun angles might be desired in buttonhook and dawn posigrade landings and will be included in the discussion.

At sun elevations of 22° or above, crater shadows will be largely or totally absent, and thus SA landings will lack one of the prime visual clues available in a SB landing at optimum sun angles, where the high contrast shadows are strikingly evident against the monochromatic lunar surface. To balance this, contrast differences between surface features are higher in general in a SA landing than they are for the corresponding sun elevation in a SB landing, as is shown in Section 4.1. Shadows cast by steep-sided rock outcrops will still be visible as well, perhaps more visible than in a SB landing where they are partially occulted.

The lunar terrain appears from two to eight times darker in a SA landing than in a SB landing and tends to darken near the horizon, whereas with the sun behind the LM the terrain grows brighter near the horizon, especially in the washout area. It is never really very bright in either case, however, since the albedo of the lunar maria is only about 7%, about that of dark volcanic rock. Since the sun might be shining in the astronaut's eyes in a SA landing the terrain could appear even darker than the reflection characteristics of the lunar surface indicate, due to the change in the eye's adaptation level. Such differences in terrain brightness between the two types of approach are not

*Angles are defined in Figure 5.

considered significant, but the fact that the sun is visible in a SA landing is highly important. The sun is a light of exceedingly great brilliance, 2.1×10^{8} cd/ft^2 luminance, and very small angular area, 6.8×10^{-5} steradians, in an otherwise black sky - a very powerful source of glare.

3.0 ANALYSIS OF LUNAR GLARE

3.1 Visibility and Contrast under Glare Conditions

Since the lunar landscape is nearly monochrome, the principal clue for the detection of obstacles is the contrast they and their shadows make with the surrounding surface. In the following discussion it will be found useful to adopt a somewhat standard terminology and refer to any object at the landing site, be it crater, boulder, shadow, or difference in slope, as the target. The smallest targets of interest at any altitude can be thought of as roughly .5 degree in diameter, half a fingernail's width at arm's length. The surface adjacent to the target, out to about a 2 degree diameter, is called the background, while the remainder of the field of view is called the surround. In this paper, the portion of the LM commander's window which covers the target and background, as shown in Figure 3, is named the Active Scattering Area (ASA). It is about a half inch in diameter.

Glare has three major components. Dazzle glare, the first of these, is a phenomenon peculiar to the eye, which makes perception of an object more difficult when a bright light such as the sun is in the field of view. Scatter glare consists of the light scattered into the line of sight by any material on an otherwise transparent window; it is external to the eye (would be photographed by a camera) as is reflection glare, which consists of all the light reflected by the window into the line of sight. Reflection glare in the LM is not treated quantitatively at much length in this paper since it is not intrinsic to the LM/lunar environment and because it is presently being reduced by modifications to the LM cabin materials.

As shown in the following sections on dazzle and scatter and reflection glare, all three effects cast a veil of brightness over the field of view. This veil increases the total luminance*

---

*Luminance, B, (also called brightness) is the luminous intensity per unit projected area of the source, while illuminance or illumination, E, is the luminous flux incident on a unit area of receptor surface.

of the scene but since it affects both target and background equally it reduces the ratio between them. Since the human eye is more sensitive to brightness ratios than to the brightness levels themselves, a veiling luminance reduces scene visibility. The common definition of contrast, due to Blackwell, is

$$C = \frac{|B_T - B_B|}{B_B} \tag{1}$$

where C is the contrast without glare, B_T is the target luminance, and B_B is the background luminance. If a veiling luminance B_{VD} due to dazzle, a veiling luminance B_{VS} due to scatter, and a luminance B_{VR} due to reflections are added, so that the target luminance is now B_{TG} and the background luminance B_A, the contrast with glare, C_G, becomes

$$C_G = \frac{|B_{TG} - B_A|}{B_A} = \frac{|(B_T + B_{VD} + B_{VS} + B_{VR}) - (B_B + B_{VD} + B_{VS} + B_{VR})|}{B_B + B_{VD} + B_{VS} + B_{VR}}$$

$$= \frac{|B_T - B_B|}{B_A} = \frac{B_B}{B_A} C \tag{2}$$

where B_A is the adaptation luminance, that is, the level of brightness to which the eye is adapted.

We may also define a relative contrast with glare or contrast ratio, C_R, and subsidiary relative contrasts in which either dazzle (C_{RD}), scatter (C_{RS}), or reflection (C_{RR}) is the only glare component:

$$C_R = \frac{B_B}{B_A} = \frac{C_G}{C} \leq 1 \tag{3}$$

$$C_{RS} = \frac{B_B}{B_B + B_{VS}} \tag{4}$$

$$C_{RD} = \frac{B_B}{B_B + B_{VD}} \tag{5}$$

$$C_{RR} = \frac{B_B}{B_B + B_{VR}} \tag{6}$$

Normally, in the following analysis B_{VR} will be assumed equal to 0 and C_{RR} equal to 1.

Then

$$\frac{1}{C_R} = \frac{1}{C_{RS}} + \frac{1}{C_{RD}} - 1. \tag{7}$$

Figure 4 is a nomograph of Equation (7) and permits easy calculation of C_R, C_{RS}, or C_{RD} when any two of these three quantities are known. C_R reduces to C_{RS} when there is no dazzle and to C_{RD} when there is no scatter glare.

The relative contrast is a measure of the degradation of vision due to glare. When there is no glare C_R is equal to 1; when the glare-generated veiling luminance is equal to the background brightness, $C_R = 0.5$. An interesting property of the relative contrast is that it can be applied to comparisons of contrast of any object with the lunar surface, even if the object does not have the same photometric properties as the surface. Thus, for example, it gives directly the apparent contrast of a lunar shadow ($C \equiv 1$) under glare conditions.

A reduction in the contrast of an object as measured by C_R may imply a reduction in the maximum range at which the target is visible. Large targets will remain visible at any range until the contrast is reduced below a critical value (the liminal contrast) and then become indetectable by luminance contrast differences. One recent lunar visibility study (Reference 31) suggests that, for a 0.5° target on the lunar surface such as is considered here, the critical contrast is 0.03.

For smaller targets it can be shown that the reduction in range (R_R), or ratio of the maximum range with glare to the range without glare, is given by

$$R_R = \sqrt{C_R} \tag{8}$$

This equation is applicable to the crater obstacles which are studied in Reference 43, where it is calculated that 20 foot diameter craters are detectable at 3000 ft. altitude (9000 ft. range) without glare. With glare, assuming C_R to be 0.5, these craters would become visible at about 6300 feet range.

Although the major emphasis in this report is on C_R, the degradation of contrast relative to that seen without glare, and on the consequent reduction in range, it will also be necessary to work with the contrast levels themselves. In order to be able to compare C_G with the contrast curves presented in Reference 27 the definition in Equation (1) of C by differences in brightness levels (difference contrast) must be modified. Given that the lunar background luminance in candles/ft^2 is

$$B_B = t_{HW} \frac{\rho_o E_o}{\pi} \Phi(\alpha, \tau) \tag{9}$$

the contrast between two contiguous surface elements with different slope can be written, as in Reference 27,

$$C = \frac{\Delta B}{B_B}$$

$$= \frac{\Delta \Phi}{\Phi_B} = \frac{1}{\Phi_B} \frac{\partial \Phi}{\partial \tau} \Delta\tau. \tag{10}$$

In these equations the combined transmission loss through the helment and window is t_{HW}; ρ_o is the normal albedo of the surface (taken as .072 throughout this report); E_o is the normal solar illuminance of 12,500 ft-cd, and α and τ are the sun-eye phase angle and the luminance longitude of the background as shown in Figure 5. $\Delta\tau$ is the difference in slope (nominally 10°) and Φ is the lunar photometric function. In this study the function due to Fedorets is used.

It is easily seen that any transmission loss through the window and helmet, if constant over the area is question, has no effect on contrast, relative contrast, and relative range, since if t_{HW} represents the combined transmission of helmet and window, then, as seen by the astronaut, the contrast with transmission loss is

$$C_t = \frac{\left| t_{HW}B_T - t_{HW}B_B \right|}{t_{HW}B_B} = C$$

The characteristics of lunar surface contrast with glare, the relative contrast, and the reduction in range are discussed further in Section 4.1 after the dazzle and scatter equations are developed.

3.2 Dazzle

The phenomenon of dazzle has been the subject of many experiments. It has been found that a strong light shining in the eye has exactly the same effect as a uniform veil of light over the observed object and its surrounding area. This "equivalent veiling luminance" B_{VD} has been found to be proportional to the normal illumination by the glare source at the eye, E_N. The luminance is essentially independent of the angular area of the dazzle source, its azimuth angle about the line of sight and the spectral composition of its light, but varies roughly as an inverse power (approximately the inverse square) of the angle θ between the line of sight and the rays from the source. That is

$$B_{VD} = k \frac{E_N}{\theta^n} \qquad (11)$$

where k and n are the experimentally derived constants of Table 1, which summarizes the conditions and pertinent results of seven experiments.

Several physiological explanations have been advanced to explain this dazzle effect. The most probable, supported by diverse experiments (Reference 6), is that the dazzle veil is generated by incident light scattered within the eye itself. (A priori, it is reasonable to expect some internal scattering since the eye is not perfectly homogeneous.)

Whatever the explanation, an examination of Table 1 reveals several characteristics of the experiments:

1. The number of subjects who participated in each study is low, typically two persons, and the variations in the derived values of k and n are probably largely caused by, and an indication of, the difference in individual ability to perceive contrast in a glare environment.

2. The intensity of the glare source used in the experiments was far below that to be encountered on the moon, i.e., a maximum of about 50 ft-cd illumination at the eye compared to a solar constant of 12,500 ft-cd.

3. The range in angle θ and background brightness B_B is adequate for application to the lunar mission.

The difference in glare source intensity might be considered a serious obstacle to extrapolation of these results to the lunar environment. However, as the dazzle mechanism is probably internal scatter, and scattering will be seen to be a linear function of the illumination, it may be expected that the veiling brightness will remain a linear function of illumination even for a very high intensity source such as the sun.

The variation in k and n is a more serious obstacle. Only two of the experimenters, Holladay (1926) and Stiles and Crawford, state the expected uncertainty of their results. Besides the variation from individual to individual, Stiles and Crawford (Reference 8) also point out a day to day variation in individual response of about 20%. This can be compared to the maximum individual deviation of 40% and average deviation of 12% in contrast sensitivity from the fitted curves reported for Blackwell's Tiffany studies (Reference 25) which are the standard source of contrast sensitivities for the non-glare situation. Such uncertainties have not been emphasized in applications of visibility studies to the lunar mission, but are obviously important in any analytical visual range estimate.

To show what this uncertainty in glare response means under lunar conditions, the solar dazzle luminance at high gate has been plotted in Figure 6 as a function of sun angle at 0° azimuth. The angles involved are defined in Figure 5 and Appendix A. It should be noted that every point in the hemisphere about the target can be referred to by two combinations of sun angle and azimuth; in particular, a sun angle of 170° at 0° azimuth is the same as a sun angle or elevation of 10° at 180° azimuth. It should also be noted that in Figure 6 a decreasing sun angle corresponds to an increasing θ. That is,

$$\theta = 180° - \text{Sun Angle} + \text{Look Angle}$$

where the look angle in Figure 6 is 14.4°.

In Figure 6 three of the dazzle models from Table 1 are shown: the Stiles (1929) model above, the Fry and Alpern model below, and the Stiles and Crawford suggested mean value

(B_{VD}) in the middle. The shading on the mean curve shows the +10% variation. A fourth dazzle curve taken from Reference 42, which will be discussed later, and a curve showing the lunar surface brightness B_B as a function of sun angle are also given.

The B_B curve acts as a reference level for the dazzle curves in the figure. The lunar surface at the target appears brightest when the target is in the washout area at a sun angle equal to the look angle. At the point the dazzle mechanism comes into play the surface appears only one tenth as bright as at washout and a small dazzle liminance has a strong effect on contrast levels. With the aid of Equation (5) and the figure it can be seen that contrast would be reduced by one half at sun angles of about 122°, 132°, and 160°, according to the curves of Stiles, Stiles and Crawford, and Fry and Alpern, respectively. The Stiles and Crawford mean values will be used in this study, as the more recent Fry and Alpern study was concerned with very small angles.

The discontinuity in the dazzle luminance curves near a sun angle of 120° is due to the shielding of the eye from the sun by the LM window rim and forward beam. The exact angle where this shielding occurs is dependent upon the eye location as well as the LM orientation; throughout this report the eye was assumed in the design eye location. Figure 7 displays the dazzle luminance cut-off angles for various LM pitch angles.

Figure 6 does not tell the full story of the effect of solar dazzle. Everyone, from their own experience, knows how painful it can be to look within 30 or 40 degrees of the sun, even though the dazzle veil may not completely wash out details in that region. The automatic response to the discomfort is to squint or shade the eyes with the hand. Since neither of these methods is really appropriate, it would be better to use an external shield. The astronaut could reduce the intensity of the light by use of his Extra Vehicular Visor Assembly (EVVA), but it would be preferable to block the light from the cabin altogether. The sun could be blocked either by varying the azimuth by 20° or more to the left of 180° as is shown by Figure 7, or by shading the upper portion of the window down to the horizon, if this is considered operationally feasible.

If dazzle glare is not prevented by some means or other, it can hinder detection of surface features to a great extent, especially for forward sun elevations less than 40° (sun angles greater than 140°). This is indicated to some extent in Figure 6, and will be shown more clearly in Section 4.1. But it would be unrealistic to reject a particular lunar descent trajectory during mission planning solely on the basis of high solar dazzle,

when dazzle will almost certainly be blocked in practice, if not by pre-mission modifications, then by the astronaut's reflexive action during descent.

3.3 Scatter

In addition to the loss in visibility due to dazzle, a further loss can occur due to any particles or films that may be deposited on the commander's window. A thick opaque mass will block the view of surface features behind it; a thinner deposit will scatter light from the sun, LM structure and lunar surface incident upon it into the commander's line of sight, creating a bright veil over the scene and lowering contrast in the manner described previously.

3.3.1 Sources of Scatter Contaminants

Several potential sources for film and particulate debris have been suggested:

1. Spacecraft/LM Adapter (SLA) pyrotechnic separation;
2. Outgassing of spacecraft materials;
3. Plume impingement from the SM-RCS;
4. Plume impingement from the LM-RCS.

In regard to the first source, pictures taken in the SLA during the flight of SA-202 had shown a large amount of debris from the detonating fuse which separates the SLA panels. However, the blast shields about the fuse have recently been redesigned and the total amount of explosive reduced so that MSC does not presently recognize any debris problem from this source (Reference 45).

So-called outgassing of materials about the window area, the second potential source of window debris, was a serious problem on several Gemini flights, notably Gemini VII and Gemini XI. On Gemini XI, for example, a clear but light-diffusing oily patch about 4 by 6 inches formed on the command pilot's window. It became more prominent during the flight and was severe enough that the command pilot had great difficulty in seeing a first-magnitude star (Reference 24). It was found that the film was composed of condensable silicone oils from the silicone gaskets and sealants around the window. Before the Gemini XII flight the gaskets were vacuum post-cured and all the excess sealants were removed from the window area. The treatment was successful and no contamination due to outgassing was noted on the last Gemini flight (Reference 10). Similar measures are being taken to forestall any such problem on the LM.

Window contamination due to RCS plume impingement, the remaining possible source listed above, was first recognized as a possible problem during investigations of ignition pressure spikes in the RCS engine chambers in tests performed at MSC, Marquardt and the Bureau of Mines in 1966 (References 11, 14, 18).

After the runs at MSC, residue forced out of the engine during the test was found on the test stand and on the ceiling above the engine. Both solid and liquid forms of the residue were observed. The liquid form of the residue ranged from quite watery to very viscous in consistency and from straw-yellow to dark brown in color. It was apparently of very low vapor pressure since some liquid was observed to remain in the engines for more than an hour at a test cell pressure of 50μ Hg with an engine temperature greater than 100°F. A solid residue, a whitish-tan crystalline material resembling brown sugar or jeweler's rouge, was also found at times on the test stand and in the nozzle extension. The liquid residue could be transformed into this solid form if held at a high vacuum (0.1μ Hg) for several hours. Tests were run with hydrazine, monomethyl hydrazine (MMH), unsymetrical dimethyl hydrazine (UDMH), and Aerozine-50 (50% hydrazine, 50% UDMH) fuels, and similar residues were found in each case. MMH was found to produce less residue than Aerozine-50 and was chosen for the SM-RCS system to reduce explosion hazards from the residue while Aerozine-50 was retained for the LM-RCS. (Inhibited nitrogen tetroxide is the oxidizer in both systems.) Analysis of the residue formed by the two fuels showed it to be principally hydrazine nitrate, in the case of Aerozine-50, and monomethyl hydrazine nitrate, in the case of MMH.

The Bureau of Mines also studied the engine residues and confirmed MSC's findings. Mr. H. Purlee of the Bureau has described the Aerozine-50 residue as a conglomerate of long needle-shaped crystals in a mother liquor, which is probably a concentrated solution of nitrates and azides or nitrites in water. Ammonium nitrate could also be present in some cases. Crystals as small as .01 mm (10μ) and as large as several inches have been observed, often appearing in stellate forms (Reference 44). (The crystal size is highly dependent on the concentration of the mother liquor, the temperature and the time since deposition. On the LM window any crystals would probably be microscopic, but the exact size would be extremely difficult to estimate.) The index of refraction of the mother liquor has never been measured, but the index of pure hydrazine nitrate crystals has been found to range between 1.45 and 1.62, depending on the crystal axis orientation (Reference 20). The scatter model developed in this report incorporates as many of these characteristics of the residue as possible.

Of the two possible sources of RCS plume contamination, the SM-RCS is of secondary importance. The -x thruster in quad A points roughly toward the commander's side of the LM. However, the commander's window is at least 18 feet away from it, and is well protected by the ascent stage structure.

A far more severe impingement problem arises from the LM's own RCS thrusters, specifically the upward (I-u) and forward (I-f) pointing thrusters in RCS quad I, which are mounted about 3-1/2 feet from the commander's window (see Figure 1). To determine the severity of this problem, an experiment (Reference 15) was conducted at MSC in February-March of 1966 to measure the loss in transmission and increase in scattered light in the window (and Alignment Optical Telescope) after exposure to thruster I-u in a complete descent/ascent sequence. Tests were carried out in the 20-foot vacuum chamber of the Auxiliary Propulsion Test Facility employing a full-scale RCS thruster. After exposure to the plume, the window samples (with both HEA and WBHM coatings) were removed from the chamber and transmission and scatter were measured with a photometer. The results showed a 25% loss in transmission through the window and an increase in scatter by a factor of 10 to 40, although total scatter was still small.

The test report states that these values are qualitative guides, rather than quantitatively accurate measures. The limited scope of the experiment did not permit control of all the environmental factors, notably humidity and temperature, that govern the optical properties of the residue. In particular, no evidence of the crystalline residue found earlier was noted during the optical tests (apparently because the hygroscopic nitrates had deliquesced in the humid atmosphere leaving only microscopic scattering centers in the liquid). The residue evaporation and crystal formation rates were probably also strongly affected by the chamber and sample temperatures, which were not at lunar mission levels (Reference 22). Nonetheless, because the liquid residue is probably a less potent scatterer than the solid form, the experimental values can probably be taken as a lower bound for window degradation. The index of refraction of the residue, which can be derived from the scatter measurements, is probably also approximately correct and provides a check point for the theoretical model.

3.3.2 The Scatter Model

A theoretical model was developed in order to include scattering effects in the study of glare and to fill the gap left by the absence of good experimental data. In brief, the model consists of a thin film of mother liquor on the outer window pane, which covers the Active Scattering Area uniformly

and has a nominal index of refraction equal to that of water ($n_F = 1.33$). Suspended at random in this film are a large number of transparent or slightly absorbent spherical scattering particles of various sizes, all of the same refractive index, n_S. The particle density per unit area is sufficiently small that multiple scattering (i.e., scattering by a particle of already scattered light) is unimportant. Both a large range in particle size and a large mean size (at least several wavelengths in diameter) are assumed, in accord with the known properties of the RCS residue. Because of the large spread in size and the random particle placement, phase effects in the light scattered by different particles will cancel and can be ignored. Thus, the total intensity of the scattered light will be the sum of the individual particle intensities.

3.3.2.1 Single Particle Scattering

Each particle in the ASA will intercept some of the incoming light and scatter it over a whole sphere, the intensity in any direction being in accord with the scattering law for that particle. Figure 8, which includes polar scatter plots for five particles of different diameters, demonstrates how greatly the intensity can vary with a small change in size. The diagrams also show the series of maxima and minima which appear when the particles are about a wavelength (.555 μ) in circumference and which become increasingly numerous as the size grows still larger. With the increase in size, the scattered light is more and more concentrated in the forward direction and the total flux scattered increases enormously. These last two characteristics are not too evident from the diagrams, which are not drawn to the same scale; however, the forward ($\theta = 0°$) intensity of the largest particle is about 10^6 times that of the particle one tenth its diameter.

The fact that the scatterers are in the present case considerably larger than a wavelength of light, permits a considerable simplification in the form of the scattering law. Instead of the rigorous expression derived by Mie in 1908 from Maxwell's equations, it is possible to use a classical approximation to it, which expresses the total scattered intensity as the sum of the light diffracted, reflected, and refracted (without internal reflection) by the particle. The work of Bricard (Reference 33) and of Hodkinson and Greenleaves (Reference 13) has shown that this approximation is valid within roughly 10% for particles larger than 3 or 4 wavelengths (1.5-2 μ) if there is also at least a 2 to 1 range in particle size to smooth out phase effects.

The use of spherical scatters in the model, where the residue crystals are described as needle-shaped, is a further approximation. However, it has been shown (Reference 23) that the average diffraction and reflection of a large monodisperse (uniform sized) ensemble of randomly-oriented particles will not differ from that of a mass of spheres of equal projected area. Even for polydispersions, Donn and Powell et.al (Reference 12, 19) have proven that it is possible to find a size distribution of spheres which scatter approximately like the set of irregular particles, at least at one wavelength or over a restricted range of θ. And since refraction from needles can be expected to be more sharply peaked in the forward direction than that from spheres, use of a sphere model in the lunar glare analysis will result, if anything, in conservatively low calculated contrasts over the range of θ of interest.

With these assumptions, the intensity of the scattered light at an angle θ due to a single particle illuminated by an incident plane wave can be written as

$$i(\theta,x,n_s) = \left(\frac{\lambda^2 x^2 E_o}{4\pi}\right) \cdot R \cdot [D(\theta,x) + F(\theta,n_s) + R(\theta,n_s) + P(\theta,x,n_s)] \quad (12)$$

The first factor, $\lambda^2 x^2 E_o/4\pi$, is simply the incident flux on the particle: the incident illumination E_o (flux/unit area) times the cross sectional area of the spherical particle, expressed here in terms of the size parameter $x = \pi d/\lambda$, where d is the diameter and λ is the wavelength of the incident light. The second factor is the Rayleigh function, $R = \frac{1 + \cos^2\theta}{2}$, where θ is measured from the forward direction.

The D term inside the brackets is the well-known Airy diffraction formula

$$D(\theta,x) = \frac{x^2}{4\pi} \left[\frac{2 J_1(x \sin\theta)}{x \sin\theta}\right]^2 \quad 0 < \theta < \pi/2 \quad (13)$$

where J_1 is the Bessel function of order 1.

F and R are the reflection and refraction components, respectively, which were first derived by Wiener in 1907. They can be written, in Hodkinsons' formulation (Reference 13) as

$$F(\theta,n_S) = \frac{1}{8\pi}\left\{\left(\frac{\sin\psi - f}{\sin\psi + f}\right)^2 + \left(\frac{n_S^2\sin\psi - f}{n_S^2\sin\psi + f}\right)^2\right\} \qquad (14)$$

$$R(\theta,n_S) = \frac{2}{\pi}\left(\frac{n_S}{n_S^2-1}\right)^4 \frac{(n_S\cos\psi - 1)^3\,(n_S - \cos\psi)^3}{\cos\psi\,(n_S^2 - 2n_S\cos\psi + 1)^2}\,(1 + \sec^4\psi) \qquad (15)$$

where $\psi = \theta/2$,

and $f = [n_S^2 - 1 + \sin^2\psi]^{1/2}$

It is important to note that D is a function of the size of the particle but not of its index of refraction, while F and R are functions of the index of refraction but not of the size. P, the last term, is a function of both. P represents the phase effects between the diffracted, reflected, and refracted rays. In a polydispersion, Bricard has shown that only the interference between the diffracted and reflected waves is important, and P becomes in that case,

$$P(\theta,x,n_S) = \frac{c}{\pi}\sin(\delta x)J_1(z) \qquad (16)$$

where

$$z = x\sin\theta$$

$$\delta = 2\sin(\theta/2)$$

$$c = 4[r(n_S)]^{1/2}\,\frac{\cos^2(\theta/2)}{\sin\theta}$$

and $r(n_S)$ is the reflectance of the particle calculated by the standard Fresnel formula

$$r(n_S) = \frac{\sin^2(\theta - \theta')}{\sin^2(\theta + \theta')} + \frac{\tan^2(\theta - \theta')}{\tan^2(\theta + \theta')}$$

where

$$\sin\theta' = \frac{n_F}{n_S} \sin\theta$$

n_F being the index of refraction of the film of mother liquor.

P is only important for small scatterers, since in large ones the diffracted component is nearly zero except for $\theta \approx 0$ (where the classical approximation is invalid in any case).

3.3.2.2 Particle Size Distribution

In order to determine the total intensity of the scattered light from all the particles in the ASA, their size distribution must be taken into account. It was not considered feasible to attempt to derive the distribution from first principles, given the number of factors governing particle growth in this case. Instead, the particle number density was assumed to be a negative exponential function of the size parameter. The negative exponential distribution exhibits the proper physical characteristics that experience with small particle distributions leads one to expect: small particles are more numerous than large ones and sizes are distributed in a skewed unimodal curve. A modified lognormal function, such as the Upper Limit Equation of Mugele and Evans (Reference 17) might have somewhat more theoretical justification, but would not permit a closed form solution for the scattered intensity. Given the expected accuracy of the experimental data to which the model was fitted, the use of the Upper Limit Equation was not considered warranted. Also, due to the relatively large size of the scattering particles, errors in estimating the particle size and size distribution were not expected to be significant over the range of θ of interest in this study. To check this assumption, the scattered intensity of a uniform distribution was also calculated.

As shown in Appendix B the total intensity at angle θ from the forward direction of the sun light scattered by the particles in the ASA can be written for any distribution as

$$I(\theta) = E_o a_{TOT} \left[F + R + \frac{1}{\bar{a}} \int_{\text{all } x} \{D(x) + P(x)\}\, a(x) p(x) dx \right] \qquad (17)$$

where a(x) is the cross-sectional area of a particle with size parameter x, p(x) is the probability density function for the size distribution chosen,

$$\bar{a} = \int a(x)p(x)dx$$

is the mean cross-sectional area of the particles in the ASA, and a_{TOT} is the total cross-sectional area of the ensemble of particles.

For the uniform distribution, with P = 0 and the approximations given in Appendix D, Equation (17) becomes

$$I(\theta) = \begin{cases} E_o a_{TOT} \left[F+R + \dfrac{R}{\pi \sin^4 \theta} \dfrac{3}{4x^2_{mean}} \right] & \sin\theta \geq 1.5/x \qquad (18\text{-A}) \\ E_o a_{TOT} \left[F+R + \dfrac{3x^2_{mean}}{5\pi} \right] & \sin\theta < 1.5/x \qquad (18\text{-B}) \end{cases}$$

x_{mean} being the size parameter of the particle of mean diameter.

For the negative exponential distribution the intensity Equation (17) becomes

$$I(\theta) = E_o a_{TOT} \left[F+R + \frac{4q^3}{\pi} \left\{ \frac{Rk^3}{4\pi\beta^5} \left(\frac{(1-k^2)K-(1-2k^2)E}{(1-k^2)} \right) + \frac{3\beta\mu}{\kappa^{5/2}} \sin(\xi - 5/2\ \eta) \right\} \right] \qquad (19)$$

where 2q is the parameter of the negative exponential distribution

($x_{mean} = \frac{1}{2q}$). K and E are the complete elliptic integrals of the first and second kinds, respectively, and k is their modulus. The variables β, μ, κ, ξ, and η are auxiliary functions of θ defined in Appendix C.

3.3.2.3 Luminance of the ASA

Once the scattered intensity has been calculated according to the above formulae, the luminance of the ensemble of particles, B_S, follows directly. By definition $B_S = I(\theta)/A_{proj}$ where A_{proj} is the area of the ASA projected normal to the line of sight. But if A_o is the area of the ASA when the line of sight is normal to the window and $A_o/\cos\phi$ the area when the line of sight is at any angle ϕ from the normal (Figure 3), then

$$A_{proj} = A_o$$

and

$$a_{TOT} = \sigma A_o/\cos\phi \tag{20}$$

The scattering coefficient σ defined by Equation (20) is seen to be the ratio of the total geometrical cross sectional area of the scattering particles to the area of the ASA. This definition differs from the more usual definition of the scattering coefficient, σ_o, which is the ratio of the sum of the scattering cross sections of all the particles to the area of the ASA, or equivalently, the ratio of the total scattered flux to the total incident flux. This last definition is the one used in the previous LM glare analysis, Reference 42, which is discussed below. The ratio of σ_o to σ is the average scattering efficiency coefficient of the distribution, and for the range of particle size considered in this study is approximately equal to 2.

Using σ, B_S then becomes

$$B_S = \frac{\sigma E_o}{\cos\phi} [I] \tag{21}$$

where [I], scattered intensity/incident flux, is the portion of

$I(\theta)$ in Equations (18a), (18b), and (19) enclosed in square brackets. The scatter veiling luminance, B_{VS}, can be found from B_S once the effects of the film in which the particles are considered embedded are determined.

3.3.2.4 Film Effects

Due to its (nominal) index of refraction $n_F = 1.33$ and transmission, t, the film has six effects on the scattered light:

1. The relative index of refraction of the particles to the surrounding medium is reduced: $n_S \rightarrow n_S/n_F$;

2. The wavelength of light is reduced: $\lambda \rightarrow \lambda/n_F$;

3. The intensity of the scattered light is decreased by the amount (1-t) absorbed or reflected by the film;

4. The scattering angle θ is smaller inside the film than the value measured outside;

5. The solid angle containing the scattered flux is smaller inside the film than outside and the intensity is consequently greater;

6. The incident beam is broaded inside the film, and the illumination on the scatterers is consequently less.

The evaluation of effects 5 and 6 may be found in Reference 21; effect number 4 is a straightforward application of Snell's law.

3.3.2.5 Scatter Characteristics

In order to give an idea of the relative contribution of reflection, refraction, and diffraction plus phase effects in the two distributions, Figure 9 was prepared. The cases shown include four combinations of scatterer index of refraction and mean diameter for the exponential distribution (models w, x, y, z) and two of the same combinations for the uniform distribution (models u, v). The values chosen represent the expected maxima and minima for the window residue, and the plots are arranged from top to bottom in order of increasing effect on lunar surface contrast as found by comparison of the corresponding C_{RS}.

It can be seen that the major reason for the decrease in relative contrast is the widening of the forward lobe as the index of refraction increases and the size decreases. Five other characteristics of the scatter intensity are notable:

1. The wide range of sizes in the polydispersion has supressed the extreme irregularity visible in the single-particle scatter curves of Figure 8;

2. Diffraction in the uniform distribution is more peaked than in the exponential distribution because of the greater influence of larger particles;

3. Diffraction in both models is extremely peaked about $\theta=0$ and is unimportant for $\theta \gtrsim 10°$, hence

4. The two models are equal for $\theta \gtrsim 10°$, and finally

5. Reflection is insignificant compared to the other effects.

Refraction is the major scatter generator over most of the angular range of interest. Therefore, it can be expected that the index of refraction will be the critical parameter and that neither the exact mean size nor the exact size distribution will be of great importance.

3.3.3 Fitting of the Scattering Model to the MSC Data

Since the MSC results (Reference 15), though mostly qualitative, are the only experimentally derived information available of LM window scatter, an attempt was made to fit the model to the experimental data to derive bench mark values of σ, n_S, and d_{mean}. The following cases were tested:

1. Uniform distribution (P=0) both with and without the liquid film

   a. Transparent particles
   b. Opaque particles (R=0)

2. Negative exponential distribution

   a. Transparent particles
   b. Large-particle bias (P=0)
   c. Opaque particles (P=0, R=0)

In general 1a and 2a fit the data best, no significant improvement being apparent in the negative exponential distribution

over the uniform distribution. The negative exponential distribution did show slightly more sensitivity to changes in particle size but, overall, the fit was equally good for any mean diameter d_{mean} from 3 to 100 microns. This is to be expected, since only angles greater than 20°, where diffraction and size effects are unimportant, were covered in the MSC data.

The presence or absence of the liquid film was found to have little effect on the results, the value of n_S which resulted in the best fit only varying by about .05 when the film effects were supressed. However, the value of n_S and σ which best fit the data did vary consistently with the coating used on the experimental window sample, perhaps indicating some residue/coating interaction; but variations with changes in light source orientation, which should be zero and imply an imperfect model fit, mask this to some extent. The best fit n_S for the WBHM coating used on the outer window is about 1.5 but values go as high as 1.62 depending on the data subset used. The index for the HEA coating is somewhat higher, 1.56. Both values of n_S agree well with the values reported for hydrazine nitrate, 1.45 to 1.62. The best value of σ lies between .002 and .005, which indicates very low scatter, much below the value assumed in earlier work on glare, σ_o = .1 or σ = .05.

These results prompted the following selection of variable ranges: n_S = 1.5 - 1.6, σ = .005 - .1, d_{mean} = 2.7μ - 66.4μ (i.e., q = .025 - .001), and the use of the negative exponential distribution in the lunar contrast study.

To show the spread in scatter glare produced by this spread in mean particle size and index of refraction, the veiling luminance B_{VS} for the four combinations of d_{mean} and n_S using the negative exponential distribution and for one combination using the uniform distribution is plotted in Figure 10. The curves are computed for both the lower and upper bounds on σ, 0.005 and 0.1. The scatter luminance for any other value can easily be estimated from these curves as σ is a strictly multiplicative factor in the scattering law.

The other lines indicated in the figure include the surface brightness curve B_B, the mean dazzle luminance curve B_{VD} from Figure 6 and the LM window scatter curve given in Reference 42. The lighting conditions are those of higate at 0° azimuth as in Figure 6. The $\pm\varepsilon_S$ values displayed in the abscissa are the percentage deviation, $\Delta B_{VS}/B_{VS}$, of the models from the mean value; they will be taken as a measure of the error in the scatter model in the estimation of error in Section 4.2.

In Figure 10, the most striking property of the scatter luminance curves is their very rapid decline with increasing angular distance from the sun (decreasing sun angle), a characteristic of larger particles. Another distinctive feature is the reasonably small spread between the models despite the wide range in the parameters. This is due to the fact that even at a sun angle of 170° the line of sight is still as much as 25° off the sunline, a region where model differences are small.

The next figure, Figure 11, which is similar to Figure 7 for dazzle, shows the cut-off angles for the scatter model due to blocking of sunlight from the ASA by the LM structure. Cut off angles are calculated for a look angle of 15° but a variation in look angle of $\pm 5°$ would produce no noticeable change. No discontinuities due to blocking are visible in Figure 10 because scatter is already low at the cut-off points.

3.3.4 Scatter of Light Reflected from the Lunar Surface

The solar illumination tacitly assumed in the development of the scatter model is not the only source of light on the scattering film. Even though the lunar albedo is only about 7%, an appreciable amount of light is reflected onto the LM window by the surface, especially at low altitudes. This light scattered by the residue on the window had been thought to be an additional potential source of glare. However, as the following analysis shows, its contribution to the veiling luminance is negligible in all cases and has been excluded from the glare model.

The illumination on the window, dE, due to an element of the surface is by definition

$$dE = B \cos \gamma \, d\omega \tag{22}$$

where B is the luminance of the surface element of solid angle $d\omega$ and γ is the angle between the window normal and the vector to the surface element. Substituting from Equation (9), this can be written

$$dE = \frac{E_o}{\pi} \rho_o \Phi(\alpha,\tau) \cos \gamma \, d\omega \tag{23}$$

where E_o is the solar illumination, ρ_o the lunar albedo and Φ the photometric function. The total illumination on the ASA

is then found by integrating over the lunar surface not blocked by the LM structure. As shown in Figure 12, the maximum lunar illumination at low gate calculated in this fashion is about 120 ft-cd or 1% of the solar illumination. The scatter this level of illumination produces is very low and can be calculated be replacing E_o by dE in Equation (21), modified for film effects, and integrating as before; it is never more than about 1 cd/ft^2.

4.0 THE GLARE MODEL

4.1 Characteristics

The characteristics of the complete glare model are shown in Figures 13 through 20. Figures 13 and 14 depict the relative and true scene contrasts with glare at higate (0° azimuth) as a function of sun angle and sun elevation. Both the contrast with dazzle and scatter (C_R, C_G) and the contrast with scatter alone (C_{RS}, C_S) are plotted for high and low scattering levels. In Figure 14 the contrast without glare is plotted as well, for reference. The shaded band about the C_R and C_G lines indicates the estimated uncertainties in the relative and true contrast (calculated in Section 4.2), while the discontinuity at about 118° is due to the dazzle cut-off. Scatter is the only source of glare at higher sun elevations and lower sun angles.* The remaining line in the figures is calculated from the glare data of Reference 42 and is discussed in Section 5.0.

The two figures display in a clearer manner the glare characteristics shown in Figure 10. Especially clear is the great influence of dazzle on contrast, even where σ is as high as 0.1. In Figure 13 it can be seen that when the sun is blocked from the eye (the C_{RS} curves) the contrast is reduced by 50% and the maximum visual range (Section 3.1) by 30% at about 22° forward sun elevation for σ = .005 and at about 44° for σ = .1. When dazzle is added, the half contrast points are reached at much higher sun elevations: 48° and 55° for σ = .005 and σ = .1, respectively, and there is much less difference between high and low scatter level contrasts.

If dazzle is excluded from the eye, the scene contrast, shown in Figure 14, is comparatively high, especially for σ as low as .005, where the contrast is greater than 0.2 at 25° forward sun elevation. Reference 31 suggests that the visibility of lunar

---

*In these, and all succeeding figures scatter is calculated as the average of the w and z models.

surface obstacles (such as a 0.5° crater) will be sufficiently good to permit a landing when the slope contrast is as low as 0.03. In the same paper, it is calculated that the minimum acceptable contrast for a lunar landing, using the more conservative assumptions of Reference 43, is about 0.07. The higher figure will be adopted, somewhat arbitrarily, as the visibility criterion in this paper, even for 0.5° craters. This conservative measure is employed in order to allow to some extent for factors, such as surface granularity, uncertainty in obstacle location, and psychological pressures, which will tend to lower obstacle visibility but whose effect is not entirely known.

Even with the high visibility threshold, it can be seen that scene contrast without dazzle (C_S) is 0.07 or above for all forward sun elevations between 20° and 60°, a 40° band, for σ less than .017, and almost as high for elevations as much as 80° above the horizon. That is, contrast is acceptable over the range of sun elevation of maximum interest. If the lower visibility threshold is used as the criterion, the contrast is adequate even when the sun is only 10° above the horizon and less than 25° from the line of sight. The contrast for lower scattering levels, such as σ = .005, is above 0.18, even at 20° forward sun elevation. This is comparable to that seen in a Sun Behind landing when the sun is 2° or 3° below the line of sight. Orbiter photographs of the wash-out area, such as in Reference 30 show that a 0.5° -1° crater is plainly visible under such conditions.

If direct sunlight strikes the eye, contrast with dazzle (C_G) worsens dramatically. Scene contrast degraded by both scatter and dazzle is less than 0.07 even for σ = .005, except for a small band of sun elevations between 40° and 48° above the forward horizon. Contrast levels are above 0.03, however, for any sun elevation above 16° (for σ = .005) or 37° (for σ = .1).

Since Figure 14 is calculated for a static viewing situation at higate, Figure 15 is included to show the contrast during the entire 2.5 minute visibility phase from higate until the landing site slides below the lower window rim 10 seconds before the hover point. Contrast without glare, with scatter alone, and with both scatter and dazzle is plotted for sun elevations of 20° and 40°.

The trajectory used is that of Reference 26. As is to be expected because of the nearly constant flight path angle, contrast at all forward sun elevations remains essentially at one level from higate to logate. This is sharply distinct from the case of those SB landings in which the sun is between 14°

and 20° from the horizon where the contrast will dip to zero as the line of sight crosses the sun line and a dogleg is necessary to improve visibility. There the band of acceptable sun angles with constant contrast is only about 8° (6° to 14°); here it may be as much as 40° or more. Depending on the value of σ, the launch window is potentially much wider for a SA landing than a SB landing.

Figures 16 and 17a and 17b are included to depict the effect of azimuth on glare contrast. Figure 16 portrays the glare contrast as a function of azimuth at higate for sun elevations of 7°, 20°, 45°, and 60°. The notch in the curves near 180° azimuth due to scatter and dazzle is quite appreciable, especially for lower sun angles. (The dashed portion of the curves indicates what the contrast would be without glare.) This figure illustrates very clearly how desirable an azimuth 20° to 30° to the left is in order to improve visibility when the sun elevation is 45° or less.

The same information is displayed more extensively in the "3-D" projections, Figures 17a and 17b. Here contrast with scatter and dazzle (the z-axis) is plotted over the whole range of sun angle and azimuth for low scatter levels in 17a and high scatter levels in 17b. Sun angle (or elevation) is measured radially from 90° at the origin to 0° at the edge of the figure and azimuth is measured clockwise about the figure from 0° to 360°. The projections were made to show the glare-affected region most clearly, although some of the contrast curves are necessarily foreshortened. Figure 17b differs from 17a in that only the glare region is shown; the contrast contours not plotted would be identical to those in 17a. The most notable features in both figures are the sudden jumps in contrast at the cut-off angles where the LM structure blocks the sunlight from the eye and window. Also prominent in the glare region is the local contrast maximum at a sun elevation of about 40° which gradually sinks down and vanishes as the azimuth moves from 180° toward 270°.

Completing the set of graphs, Figures 18, 19, and 20 are plots of the relative contrasts C_{RD} and C_{RS} as a function of sun elevation for various azimuths. Figure 18 for C_{RD} assumes a look angle of 15° but the variation caused by a $\pm 5°$ change in look angle is negligible, except in the location of the cut-off angles where the relative contrast jumps to 1.0. Similarly, Figure 19 for C_{RS} at low scatter levels and Figure 20 for C_{RS} at high scatter levels both assume a look angle of 15° and pitch angle of 40°, but the variation caused by $\pm 5°$ change in either look angle or pitch is generally less than 10%. These three figures may be used to calculate C_R with the aid of the nomograph in Figure 4.

4.2 Errors

The effect of the uncertainty in scatter and dazzle luminances on the error in relative contrast can be estimated by differentiating Equation (3) and dividing by C_R

$$\frac{\Delta C_R}{C_R} = -\frac{\Delta B_{VS}}{B_A} - \frac{\Delta B_{VD}}{B_A} + \frac{B_V}{B_A}\,\frac{\Delta B_B}{B_B} \tag{24}$$

where B_V is the glare luminance, $B_V = B_{VD} + B_{VS}$, and B_A is the adaptation luminance defined previously.

If the definitions

$$\Delta B_{VD}/B_{VD} = \varepsilon_D$$

$$\Delta B_{VS}/B_{VS} = \varepsilon_S$$

$$\Delta B_B/B_B = \varepsilon_B$$

are made, Equation (24) may be rewritten for the RMS error as

$$\varepsilon_R = \sqrt{\left(\frac{B_{VS}}{B_A}\,\varepsilon_S\right)^2 + \left(\frac{B_{VD}}{B_A}\,\varepsilon_D\right)^2 + \left(\frac{B_V}{B_A}\,\varepsilon_B\right)^2} \tag{25}$$

The RMS error resulting from the first two terms under the radical was calculated for several points and found to be a fairly constant 25%. The data point scatter in the Fedorets photometric curves can be estimated from Reference 41 at approximately 25% about the fitted curves. Neglecting systematic errors, this is taken as a first approximation to the error ε_B in surface brightness. Since $B_V \leq B_A$ in Equation (25) the RMS error in C_R which has been calculated and plotted as the dashed lines in Figure 13, is less than or equal to 35%. In Figure 14 the same percentage

errors are applied to C_G, in the absence of better information, as the minimum estimated error in the contrast with glare.*

5.0 COMPARISON WITH PREVIOUS STUDIES

There have been few previous studies which are applicable to the problem of the effects of dazzle and/or scatter glare on Apollo astronaut vision, and most of these are more concerned with star detection in space rather than lunar surface visibility. Three of the studies deal primarily with the degradation in astronomical seeing arising from scatter in the "debris comet" that forms about a manned spacecraft due to RCS firings, water dumping, and out-gassing. They are of interest here principally because of the scatter model adopted.

Ney and Huch, in the earliest paper (Reference 37), assume that the debris cloud scatters isotropically and show that the surface brightness of the cloud is proportional to the particle mass ejection rate and is independent of the size of the particles. They also mention scatter glare briefly, stating that a window surface brightness one ten-millionth that of the sun would result from a scattering of one percent of the incident light. This value is higher than that determined in the present study for the corresponding $\sigma = .005$ except where the line of sight is within about 25° of the sun.

Ney and Huch's work has been extended and elaborated by Newkirk (Reference 36). The scatter model employed in his study includes the use of Airy diffraction for large individual particles and Mie scattering for the particle distribution, which is assumed to have a power-law form. The model underestimates the reduction in star visibility noted in the Gemini program, and some discussion of other possible glare sources which might account for the discrepancy is included.

The Ball Brothers Research Corporation study of the possible sources of optical contamination of the proposed Apollo Telescope Mount (ATM) is also based on the work of Ney and Huch and uses their isotropic scattering model to determine the luminance of the cloud about the ATM (Reference 16). The number, size, distribution, and lifetime of the cloud particles

---

*Some preliminary Surveyor data is said to fit the JPL Lunar Reflectivity Model (LRM) (a later version of the photometric function) to within ±20% (Reference 38). The Fedorets function rather than the LRM was used in this study in order to be compatible with Reference 27. In any case, the slope of the fitted function, which is essential to the contrast calculation, is still uncertain.

generated by the ATM configuration are evaluated from a theoretical basis. It is concluded that scatter/absorbtion on the molecular level is neglegible and that the major threat to good seeing comes from scatter from larger particles dumped by the CSM Water Management Subsystem. Outgassing/sublimation and subsequent condensation to the optical surfaces is stated to be more serious than RCS plume contamination since, because of their low molecular weight and high vapor pressure, the RCS exhaust gases will evaporate off surfaces rather rapidly. (Direct plume impingement is not a factor here.) Based on these conclusions, the report makes several recommendations for reducing contamination, several of which, such as volatile material post-curing and the provision of covers for the optics, are applicable to the LM problem as well.

A fourth study, a summary by E. E. Luedke (Reference 32) on the degradation of Apollo optical and thermal control coatings contains a complete discussion of the sources of CM surface contamination, the major contaminant in this case being the Tower Jettison Motor plume. Some discussion of the window contaimination experienced in the Gemini, Pegasus, and Apollo flight test programs is also presented. Of greatest interest to the present study is the report of the SM-RCS contamination experiments conducted by Astrosystems International. These experiments showed that the most serious degradation occurs for normal plume impingement and that the degree of degradation varies inversely with distance from the nozzle exit plane and inversely with angular distance from the nozzle center line, thus confirming the relative unimportance of the SM-RCS contamination of the LM windows.

A more generalized study than the previous ones, a report on Apollo window degradation by W. D. Miller (Reference 34), is a systematic discussion of scatter/reflection glare due to a variety of sources and its effect on astronaut vision. A set of nomographs is included to allow calculation of degraded contrasts and ranges once the bidirectional reflectance and transmittance of the spacecraft window is determined. Several examples of the application of the graphs to typical space vision problems are also given.

The only previous work on the LM glare problem itself was carried out in the Hughes Aircraft Company study of optimum lunar lighting and was documented in the final study report (Reference 29) and in a lunar surface visibility review paper by K. Ziedman (Reference 42). The curves (modified for different transmission values) which were referred to earlier in Figures 6, 10, 13, and 14 are taken or derived from the Ziedman review.

The dazzle formula employed in the Hughes/Ziedman work was the Holladay (1927) equation as revised by Fry (Reference 1) in 1954 (although the magnitude of k for the dazzle curve, reproduced in Figure 6, seems smaller than the published value). The scatter model was not discussed in the original reports but the scatter curve, reproduced in Figure 8, is derived from the equation

$$B_{VS} = t_{HW}\, \sigma_o\, E_o \cos \gamma$$

where B_{VS} is in foot-lamberts and E_o is in foot-candles (Reference 47). The angle γ is the angle between the window normal and the vector to the sun. The combined window/helmet transmission was taken to be .72 and the scattering coefficient σ_o was assumed equal to 0.1. This form for B_{VS} presupposes that the window contaminant scatters isotropically, $E_o \cos \gamma$ being the solar illumination on the window surface at angle γ.

As can be seen in Figures 13 and 14 the use of the Hughes glare model rather than the present study's model results in a generally lower calculated contrast, even in the 20°-40° forward sun elevation region of most interest for an afternoon landing. (It should be remembered that the $\sigma = .1$ worst case value employed in the present study corresponds to $\sigma_o \simeq .2$, twice the "pessimistic, although realistic" (Reference 29) Hughes value.) If the window scatter were isotropic and if the worst case amount of residue were deposited, then as the Hughes report states, contrast levels in an against-the-sun approach would be unacceptable for all sun angles. However, as shown in Section 4.1, the model developed in this study indicates that lunar surface contrast will meet the published visibility criteria over a wide band of sun angles, especially for lower values of σ and if direct sunlight is blocked from the eye.

Robert Troester

2013-RT-srb R. Troester

Attachments:
Appendix A
Appendix B
Appendix C
Appendix D
Bibliography
Table
Figures

APPENDIX A

LIST OF PRINCIPAL SYMBOLS

A	area of ASA
ASA	Active Scattering Area on Commander's window
AZ	azimuth measured clockwise from sun
B	luminance (cd/ft^2)
C	contrast
D	diffraction term in scatter law
E	illumination (ft-cd); also, complete elliptic integral of 2^{nd} kind
E_o	solar illumination, 12500 ft-cd
F	reflection term in scatter law
i	intensity (cd) of single scatterer
I	total intensity of particle ensemble (cd)
J_1	first order Bessel function
K	complete elliptic integral of 1^{st} kind
LA	look angle between local horizontal and LOS, positive downward
LOS	line of sight to target
N	number of scatterers in ASA
P	phase effects term in scatter law
PA	pitch angle between local vertical and LM $\hat{X}$-axis, positive backward
R	range; also, refraction term in scatter law
R	Rayleigh scattering function $(1 + \cos^2\theta)/2$

SA	sun angle between rear horizon and sun line; also, Sun Ahead
SB	Sun Behind
a	scatterer cross sectional area
$\bar{a}$	mean scatterer cross sectional area
d	diameter of scatterer, microns
k	modulus of complete elliptic integrals; also, coefficient in dazzle law
n	index of refraction; also, exponent in dazzle law
p	probability density function of particle size distribution
q	parameter of negative exponential distribution
r	Fresnel's formula for reflection from a surface
t	transmission
x	size parameter = $\pi d/\lambda$
z	$x \sin\theta$
α	phase angle (between LOS and sun line)
γ	angle between outward window normal and sun line
ε	estimated error
θ	angle between direction of non-scattered light and eye = $180° - \alpha$
λ	wavelength, microns
ρ_o	luminance factor of lunar surface at normal incidence and emittance (normal albedo) = .072
σ	scattering coefficient: ratio of flux geometrically incident on scatters to total flux on ASA
σ_o	scattering coefficient: ratio of total flux scattered to total flux on ASA ($\sigma_o \approx 2\sigma$)

APPENDIX B

DERIVATION OF THE TOTAL SCATTERED INTENSITY OF A SIZE DISTRIBUTION OF PARTICLES

For simplicity in the derivation, assume an ensemble of N particles, ℓ of size parameter x_1, m of size parameter x_2, and n of size parameter x_3. Then the total intensity of the light scattered by the ensemble at an angle θ from the forward direction will be

$$I(\theta) = \ell\, i(x_1) + m\, i(x_2) + n\, i(x_3) \tag{B-1}$$

if $i(x_j)$ is the intensity at angle θ of one particle of size parameter x_j and if the scattering is incoherent.

But $i(x_j) = E_o a(x_j)[S(x_j) + C]$, that is, the incident flux $E_o a(x_j)$ (the illumination on the particle times the cross sectional area) times the sum of a size dependent factor $S(x_j)$ plus a non-size dependent factor C. Hence, with a_{TOT} the total cross sectional area of the ensemble,

$$a_{TOT} = \ell\, a(x_1) + m\, a(x_2) + n\, a(x_3) \tag{B-2}$$

$$\begin{aligned} I(\theta) &= E_o \{a_{TOT}C + \ell\, a(x_1)S(x_1) + m\, a(x_2)S(x_2) \\ &\quad + n\, a(x_3)S(x_3)\} \\ &= E_o a_{TOT} \{C + \frac{N}{a_{TOT}} [\frac{\ell}{N}(x_1)S(x_1) \\ &\quad + \frac{m}{N}(x_2)S(x_2) + \frac{n}{N} a(x_3)S(x_3)]\} \end{aligned} \tag{B-3}$$

But $\ell/N = p(x_1)$ is the probability of finding a particle of size x_1 in the ensemble, and similarly, $m/N = p(x_2)$ and $n/N = p(x_3)$. Substituting, Equation (B-3) becomes

$$I(\theta) = E_o a_{TOT} \left\{C + \frac{1}{p(x_1)a(x_1) + p(x_2)a(x_2) + p(x_3)a(x_3)}\right.$$

$$\left.\mathbf{x}[p(x_1)a(x_1)S(x_1) + p(x_2)a(x_2)S(x_2) + p(x_3)a(x_3)S(x_3)]\right\} \quad \text{(B-4)}$$

It is not strictly legitimate to extend this to a continuous distribution of particle sizes (and an infinite number of particles) since a_{TOT} must diverge as N becomes large. However, in the present case N is on the order of 10^4 or more (assuming $d_{mean} \cong 10\mu$, $\sigma \cong .01$) and the integral provides a good approximation. In the limit

$$x_i \to x$$

$$p(x_i) \to p(x)dx$$

and with

$$C = F + R$$

$$S(x) = D(x) + P(x)$$

as in the body of this report, we have finally the approximation

$$I(\theta) = E_o a_{TOT} \left\{F + R + \frac{1}{\bar{a}} \int_{\text{all } x} [D(x) + P(x)]a(x)p(x)dx\right\} \quad \text{(B-5)}$$

where

$$\bar{a} = \int_{\text{all } x} a(x)p(x)dx$$

is the mean particle cross sectional area.

APPENDIX C

NEGATIVE EXPONENTIAL DISTRIBUTION: SCATTERED INTENSITY

The probability density function with parameter 2q is

$$p(x) = 2qe^{-2qx} \quad 0 \leq x < \infty \tag{C-1}$$

With this distribution,

$$x_{mean} = 1/2q$$

The cross-sectional area is

$$a(x) = \lambda^2 x^2/4\pi$$

Hence

$$\bar{a} = \int_0^\infty a(x)p(x)dx = \frac{\lambda^2}{8\pi q^2} \tag{C-2}$$

and

$$\int_0^\infty [D(x) + P(x)]a(x)p(x)dx =$$

$$\int_0^\infty \left[\frac{RJ_1^2(\beta x)}{\pi\beta^2} + \frac{c}{\pi} J_1(\beta x) \sin(\delta x)\right] \frac{\lambda^2 x^2}{4\pi} 2qe^{-2qx} \quad dx \tag{C-3}$$

where

$$\beta = \sin\theta$$

$$\delta = 2 \sin(\theta/2)$$

$$c = 4[r(n_s)]^{1/2} \cos^2(\theta/2)/\sin\theta$$

The integral of the first term

$$I_1 = \frac{\lambda^2 qR}{2\pi^2\beta^2} \int_0^\infty e^{-2qx} J_1^2(\beta x) x^2 dx \tag{C-4}$$

is an integral of the form of Equation 13.23(1) in Watson (Reference 40) and can be reduced to the form

$$I_1 = \frac{\lambda^2 qR}{2\pi^2\beta^2}\,\frac{3\beta^2}{4\pi}\int_0^{\pi/2}\frac{\cos^2 g}{(q^2+\beta^2\cos^2 g)\sqrt{q^2+\beta^2\cos^2 g}}\,dg \qquad (C\text{-}5)$$

which, with a little manipulation, can be written

$$I_1 = \frac{\lambda^2 qR}{2\pi^2}\,\frac{3k^5}{4\pi\beta^3}\int_0^{\pi/2}\frac{\cos^2 g}{\Delta^5}\,dg \qquad (C\text{-}6)$$

a standard elliptical integral

where

$$k^2 = \beta^2/(q^2+\beta^2)$$

and

$$\Delta^2 = 1 - k^2\sin^2 g$$

Finally

$$I_1 = \frac{\lambda^2 qR}{2\pi^2\beta^2}\,\frac{3k^5}{4\pi\beta^3}\left[\frac{(1-k^2)K - (1-2k^2)E}{3k^2(1-k^2)}\right] \qquad (C\text{-}7)$$

where K and E are the complete elliptic integrals of the first and second kinds, respectively, with modulus k.

The integral of the second term

$$I_2 = \frac{\lambda^2 qc}{2\pi^2}\int_0^\infty e^{-2qx}\,J_1(\beta x)\,x^2\sin(\delta x)\,dx$$

$$= \frac{\lambda^2 qc}{2\pi^2}\,\mathrm{Im}\left(\int_0^\infty x^2 e^{-\zeta x}J_1(\beta x)\,dx\right) \qquad (C\text{-}8)$$

where $\zeta = 2q - i\delta$

The integral is in the form of Watson's 13.2(6)

Hence

$$I_2 = \frac{\lambda^2 qc}{2\pi^2} \text{ Im} \left(\frac{3\beta\zeta}{(\zeta^2+\beta^2)^{5/2}} \right) \tag{C-9}$$

Given that

$$\mu = [4q^2 + \delta^2]^{1/2}$$

$$\kappa = [(4q^2 - \delta^2 + \beta^2)^2 + 16q^2\delta^2]^{1/2}$$

$$\xi = \tan^{-1}(-\delta/2q)$$

$$\eta = \tan^{-1} \left(\frac{-4q\delta}{4q^2 + \beta^2 - \delta^2} \right)$$

I_2 becomes

$$I_2 = \frac{\lambda^2 qc}{2\pi^2} \text{ Im} \left(\frac{3\beta\mu e^{i\xi}}{\kappa^2 e^{i2\eta}(\kappa e^{i\eta})^{1/2}} \right) \tag{C-10}$$

or

$$I_2 = \frac{\lambda^2 qc}{2\pi^2} \text{ Im} \left(\frac{3\beta\mu}{\kappa^{5/2}} \exp[i(\xi - 5/2\eta - m\pi)] \right)$$

where m is an integer or zero.

Hence

$$I_2 = \frac{\lambda^2 qc}{2\pi^2} (-1)^m \frac{3\beta\mu}{\kappa^{5/2}} \sin(\zeta - 5/2\eta) \tag{C-12}$$

But for very large q the major contribution ot the integral arises from small values of x before the first zero of $J_1(\beta x)\sin(\delta x)$ in Equation (C-8) where the integrand is positive. Hence I_2 must be positive and m is therefore zero.

The total intensity is then

$$I(\theta) = E_o a_{TOT} \left[F + R + \frac{4q^3}{\pi} \left\{ \frac{R\, k^3}{4\pi\beta^5} \left(\frac{(1-k^2)K - (1-2k^2)E}{(1-k^2)} \right) + \frac{3\beta\mu c}{\kappa^{5/2}} \sin(\xi - 5/2\eta) \right\} \right] \qquad \text{(C-13)}$$

APPENDIX D

UNIFORM DISTRIBUTION: SCATTERED INTENSITY

The probability density function is

$$p(x) = \begin{cases} \dfrac{1}{x_2 - x_1} & x_1 \leq x \leq x_2 \\ 0 & x < x_1,\ x > x_2 \end{cases} \qquad \text{(D-1)}$$

and

$$a(x) = \lambda^2 x^2 / 4\pi$$

$$\beta = \sin\theta$$

$$z = \beta x$$

To simplify the calculations, five assumptions are made

1. $P(x) = 0$

2. $D(x) \simeq \begin{cases} \dfrac{2R\sin^2(z - \pi/4)}{\pi^2 \beta^3 x} & z \geq 1.5 \\ \dfrac{x^2}{4\pi} & z < 1.5 \text{ (in the central maximum)} \end{cases}$

3. $(x_2 - x_1)\sin\theta = m\pi$, m a positive integer

4. $x_2 \sin\theta = (\dfrac{2n + 1}{2})\pi$, n a positive integer

5. $x_1 << x_2$ (implying $x_{mean} \simeq .5\ x_2$)

Then

$$\bar{a} \simeq \int_{x_1}^{x_2} a(x)p(x)dx = \frac{\lambda^2}{3\pi} x^2_{mean} \qquad (D-2)$$

and

$$\int_{x_1}^{x_2} D(x)a(x)p(x)dx = \begin{cases} \dfrac{\lambda^2 R}{4\pi^2 \sin^4\theta} & z \geq 1.5 \\ \dfrac{\lambda^2}{5\pi^2} x^4_{mean} & z < 1.5 \end{cases} \qquad (D-3)$$

Hence

$$I(\theta) \simeq E_o a_{TOT} \left[F + R + \begin{cases} \dfrac{3R}{4\pi \sin^4\theta} \dfrac{1}{x^2_{mean}} & z \geq 1.5 \\ \dfrac{3}{5\pi} x^2_{mean} & z < 1.5 \end{cases} \right] \qquad (D-4)$$

BIBLIOGRAPHY

Dazzle

1. Fry, G. A., "A Re-evaluation of the Scattering Theory of Glare", Illum, Eng. Symp. on Light and Vision (Feb. 1954) 98-102.

2. Fry, G. A., and Alpern, M., "Effect of a Peripheral Glare Source upon the Apparent Brightness of an Object" J. Opt. Soc. Am. 43, 3 (March 1953) 189-195.

3. Holladay, L. L., "The Fundamentals of Glare and Visibility", J. Opt. Soc. Am., 12, 4 (April 1926) 271-319.

4. ——— "Action of a Light Source in the Field of View in Lowering Visibility" J. Opt. Soc. Am., 14, 1 (Jan. 1927) 1-15.

5. Luckiesh, M., and Holladay, L. L., "Glare and Visibility", Trans. I. E. S. 20, (1925) 221.

6. Rushton, W. A. H., and Grubisch, R. W., "Glare: Its Measurement by Cone Thresholds and by the Bleaching of Cone Pigments", J. Opt. Soc. Am. 56, 1 (Jan. 1966) 104-110.

7. Stiles, W. S., "The Effect of Glare on the Brightness Difference Threshold", Proc. Roy. Soc. B104 (1929) 322.

8. Stiles, W. S., and Crawford, B. H. "The Liminal Brightness Increment for White Light for Different Conditions of the Foveal and Parafoveal Retina", Proc. Roy. Soc. B116 (1934) 55.

9. ——— "The Effect of a Glaring Light Source on Extrafoveal Vision", Proc. Roy. Soc. B122 (1937) 255-280.

Scatter

10. Blome, J. C., and Upton, B. E., "Gemini Window Contamination Due to Outgassing of Silicones", in Science of Advanced Materials and Process Engineering Series vol. II, Western Periodicals Co., 1967, 217-225.

11. Chaffee, N., and Wiltz, J. A., "Manned Spacecraft Center's Experience with Vacuum-Ignition Phenomena in Bipropellant Reaction Control Engines "AIAA Paper No. 67-514 presented at AIAA Third Propulsion Joint Specialist Conference, Washington, D. C./July 17-21, 1967.

12. Donn, B., and Powell, R. S., "Angular Scattering from Irregularly Shaped Particles with Application to Astronomy" in Kerker,M. (ed.) ICES Electromagnetic Scattering, New York: The Macmillan Company, 1963, 151-158.

13. Hodkinson, J. R., and Greenleaves, I., "Computations of Light Scattering and Extinction from Spheres According to Diffraction and Geometrical Optics, and Some Comparisons with the Mie Theory", J. Opt. Soc. Am., 53, 5 (May 1963) 577-588.

14. Juran, W., and Stechman, R. C., "Ignition Transients in Small Hypergolic Rockets", AIAA Paper No. 67-515, presented like (11).

15. Lee, J. N., "Apollo Thruster Residue Evaluation "NASA MSC Internal Memorandum CF325-6M-151, April 12, 1966.

16. McPherson, D. G., "ATM Contamination Study" Ball Brothers Research Corp. NASA Contractor Report CR-61173, May 25, 1967.

17. Mugele, R. A., and Evans, H. D., "Droplet Size Distribution in Sprays" Indust. and Eng. Chem. 43, 6 (June 1951) 1317-1324.

18. Perlee, H. E., Christos, T., and Miron, Y., "Preignition Phenomena in Small A-50/NTO Pulsed Rocket Engines" AIAA Paper No. 67-516, presented like (11).

19. Powell, R. S., Circle, R. R., Vogel, D. C., Woodson, P. D., and Donn, B., "Optical Scattering from Non-Spherical Randomly-Aligned, Polydisperse Particles" Planet. Space Sci. 15 (1967) 1641-1652.

20. Robinson, R. J., and McCrone, W. C., "Hydrazine Nitrate (1)", Analyt. Chem. 30, 5 (May 1958) 1014-1015.

21. Stein, R. S., and Keane, J. J., "The Scattering of Light from Thin Polymer Films, 1. Experimental Procedure", J. Polymer Sci., 17 (1955) 21-44.

22. Troester, R., "A Proposal for a New LM Window/RCS Plume Residue Experiment - Case 310", Bellcomm Memorandum for File, Nov. 13, 1967.

23. Van de Hulst, H. C., Light Scattering by Small Particles New York: Wiley, 1957.

24. "Gemini Program Mission Report: Gemini XI (U)" NASA MSC Report MSC-G-R-66-8, October 1966 (the section quoted is unclassified).

General

25. Blackwell, H. R., "Contrast Thresholds of the Human Eye" J. Opt. Soc. Am., 1946, 36, 624-643.

26. Alphin, J. A., Taylor, B. G., and Kirkland, B. G., "LM Powered Descent Trajectory for the Apollo Lunar Landing Mission", MSC Internal Note 68-FM-78, March 29, 1968.

27. Anselmo, D. R., and Cavedo, P. A., "Evaluation of Lunar Lighting Constraint Based upon Photometric Derived Scene Contrast" Bellcomm Technical Memorandum 66-2013-1, April 29, 1966.

28. Born, M., and Wolf, E., Principles of Optics, New York: Pergamon Press, 1959, p. 652.

29. Feng, T. Y., "A Study to Determine Optimum Lunar Lighting Conditions for Visual Selection of LEM Touchdown Point: Final Report" Hughes Aircraft Co. Report SSD 60293 R, January 1967.

30. Hamza, V., "Review of Lighting and Visual Conditions on the Lunar Surface for the Early Apollo Landing Missions-Case 340" Bellcomm Memorandum for File, May 9, 1968.

31. Heap, F., "Efficacy of Dogleg Maneuvers in Improving Visibility in LM Descent" Bellcomm Technical Memorandum 68-2013-2 June 25, 1968.

32. Luedke, E. E., "Summary Report on Optical and Thermal Control Coatings Degradation of the Apollo Spacecraft" TRW Systems Report No. 05952-6182-R00, October 31, 1967.

33. Middleton, W. E. K., Vision Through the Atmosphere, University of Toronto Press, 1958.

34. Miller, W. D., "Apollo Window Degradation", TRW Systems Report 66-3331.11-u-25, September 2, 1966.

35. Moon, P., The Scientific Basis of Illuminating Engineering, Dover, 1961, p. 420.

36. Newkirk, G., Jr., "The Optical Environment of Manned Spacecraft", Planet. Spac Sci., 15 (1967) 1267-1285.

37. Ney, E. P., and Huch, W. F., "Optical Environment in Gemini Space Flights" Science 153 (July 1966) 297-299.

38. Rennilson, J. J., Holt, H. E., and Morris, E. C., "In Situ Measurements of the Photometric Properties of an Area on the Lunar Surface", J. Opt. Soc. Am. 58, 6 (June 1968) 747.

39. Slayton, D. K. "LM Lighting/Reflection Review" NASA MSC Internal Memorandum CF 234-7M-104 (unsigned draft, no date).

40. Watson, G. N., A Treatise on the Theory of Bessel Functions, Cambridge University Press, 1962, Second edition.

41. Willingham, D., "The Lunar Reflectivity Model for Ranger Block III Analysis", JPL Technical Report No. 32-664 Nov. 2, 1964.

42. Ziedman, K. "Lunar Surface Visibility" TRW Systems Report 05952-6011-R000, August 19, 1966.

43. ——— "Visibility During Lunar Landing" TRW Systems Report 05952-6195-R000, January 19, 1968.

44. Telcons with Mr. H. Purlee, Bureau of Mines, Pittsburgh, Sept. 25, 1967, Aug. 28, 1968.

45. Telcon with Mr. R. McSheehy, NASA MSC Propulsion and Power Division, April 3, 1968.

46. Telcons with Mr. C. Wheelwright, NASA MSC Flight Crew Support Division Oct. 6, 1967, July 17, 1968.

47. Telcon with Mr. K. Ziedman, TRW Systems, Redondo Beach, Calif.

TABLE I

COMPARISON OF EXPERIMENTAL DAZZLE STUDIES

NAME (DATE)	REFERENCE	NO. OF SUBJECTS	BACKGROUND LUM. (CD/FT^2)	GLARE ILLUM. E OR E_N (FT-CD)	ANGLE (DEG) BETWEEN GLARE SOURCE AND TARGET AT EYE	$\frac{k}{CD/FT^2 - DEG^n}$ FT-CD	n	COMMENTS
LUCKIESH AND HOLLADAY (1925)	5	-	.03-30	0-9.3	5-30	12.7	2	
HOLLADAY (1926)	3	2-8	.01-150	1-20	6-20	13.7±1.6	2	EXTENSIVE, HISTORIC STUDY
HOLLADAY (1927)	4	2	10^{-5}-1	.025-.6	2.5-25	9.25	2	
STILES (1929)	7	2-4	0-.22	0-1	1-10	7.0	1.8	k, n CORRECTED IN 1937 TO VALUES SHOWN
STILES AND CRAWFORD (1934)	8	-	0-500	0-50	-	11.5	2.1	
STILES AND CRAWFORD (1937)	9	2	0	$3x10^{-6}$-20	1-105	16 (6.03 TO 27.6)	2 (1.77 TO 2.35)	MONOCULAR, EXTRAFOVEAL VISION, USES E_N
						10	2	SUGGESTED MEAN
FRY AND ALPERN (1953)	2	2-4	0	$2x10^{-3}$-34	.75-4.5	7.1	2.5	MONOCULAR, SMALL ANGLE
					MEAN VALUE (EXCLUDING FRY AND ALPERN)	10.2	2.1	

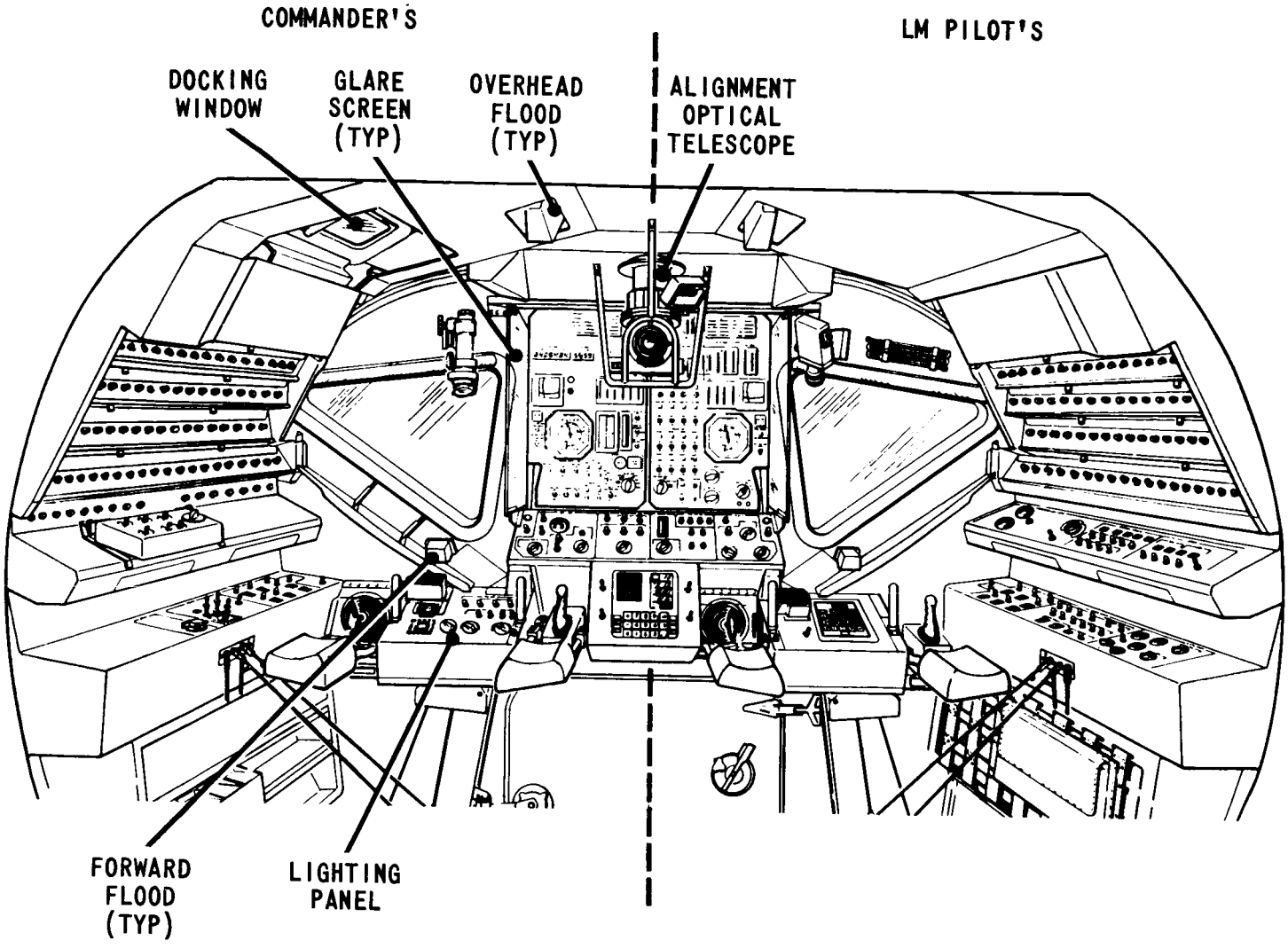

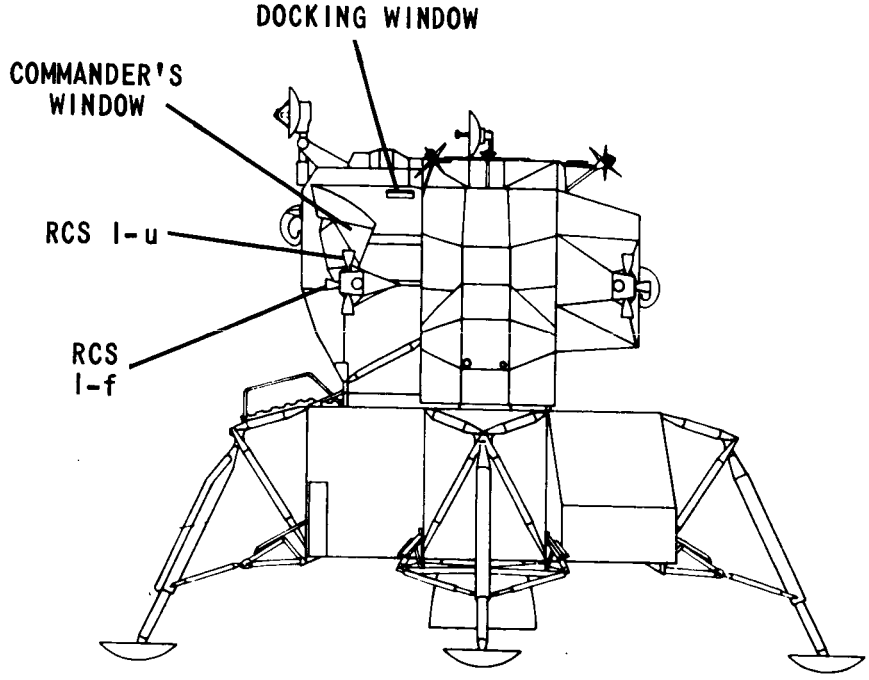

FIGURE 1 - LUNAR MODULE. INTERIOR AND EXTERIOR VIEWS.
ADAPTED FROM LM-3 APOLLO OPERATIONS HANDBOOK

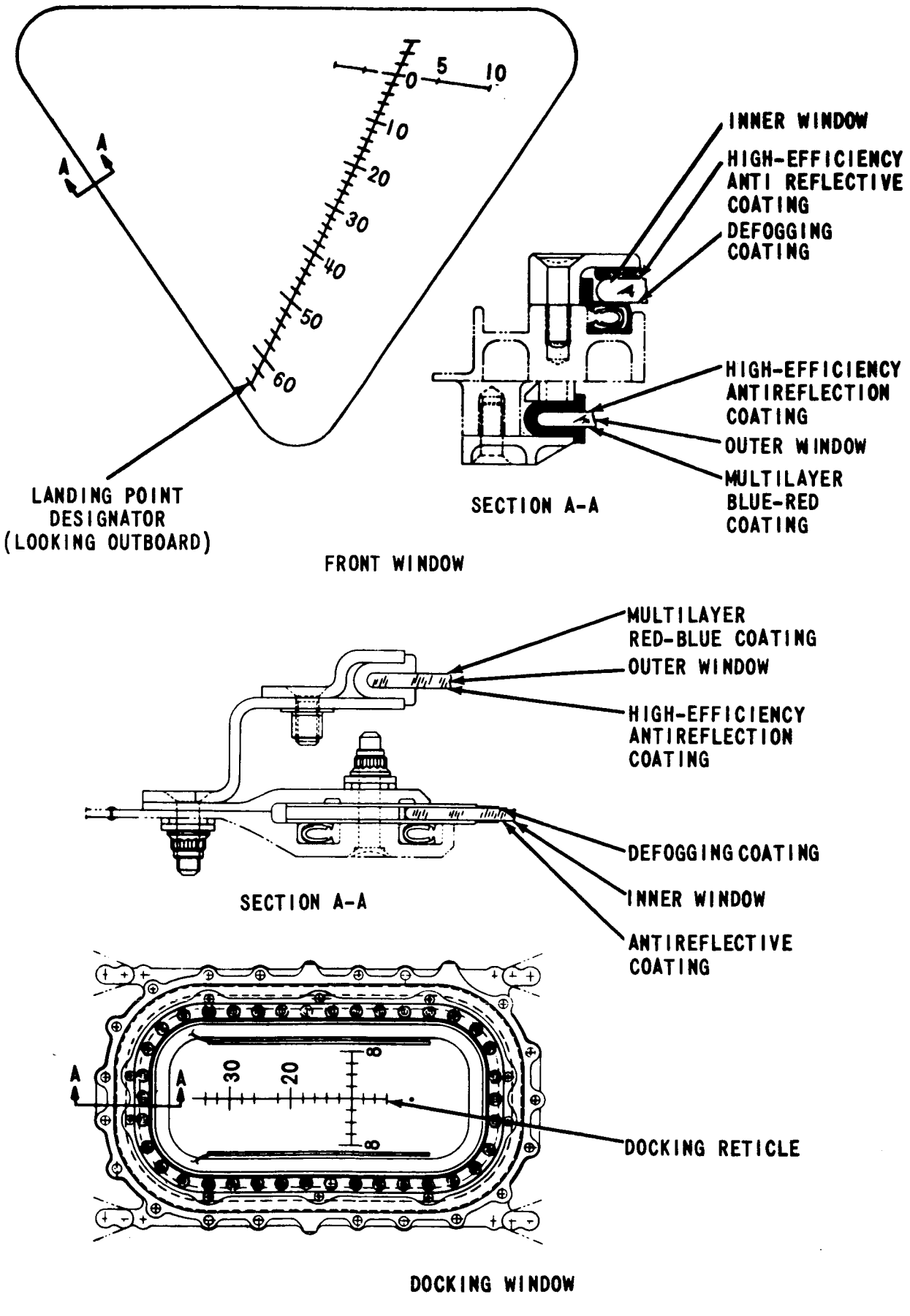

FIGURE 2 - LM WINDOW CONFIGURATION (ADAPTED FROM LM-3 APOLLO OPERATIONS HANDBOOK)

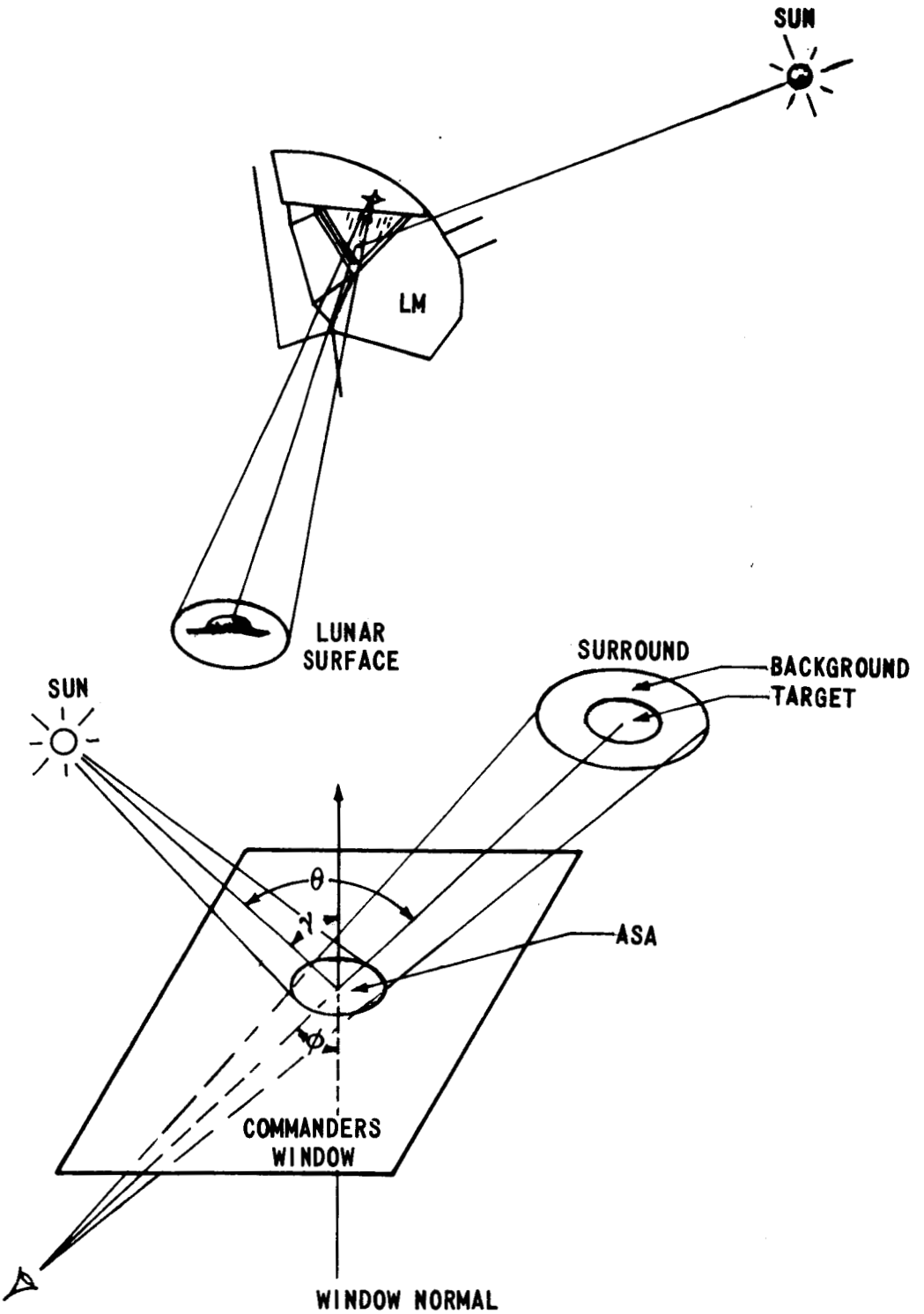

FIGURE 3 - EYE-SUN-TARGET GEOMETRY IN RELATION TO THE LM WINDOW SHOWING THE ACTIVE SCATTERING AREA (ASA)

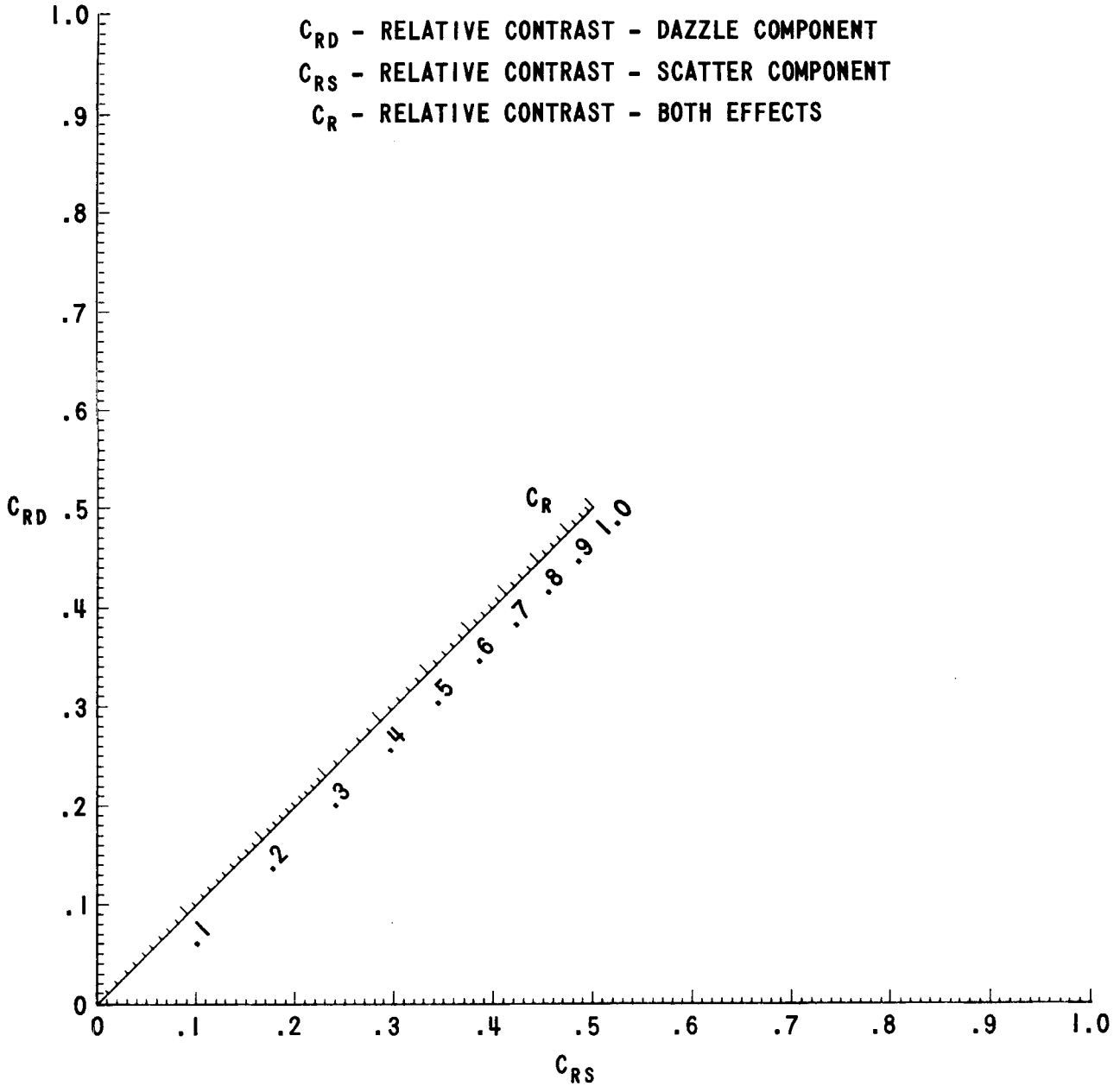

FIGURE 4 - RELATIVE CONTRAST NOMOGRAPH FOR $\frac{1}{C_R} = \frac{1}{C_{RS}} + \frac{1}{C_{RD}} - 1$

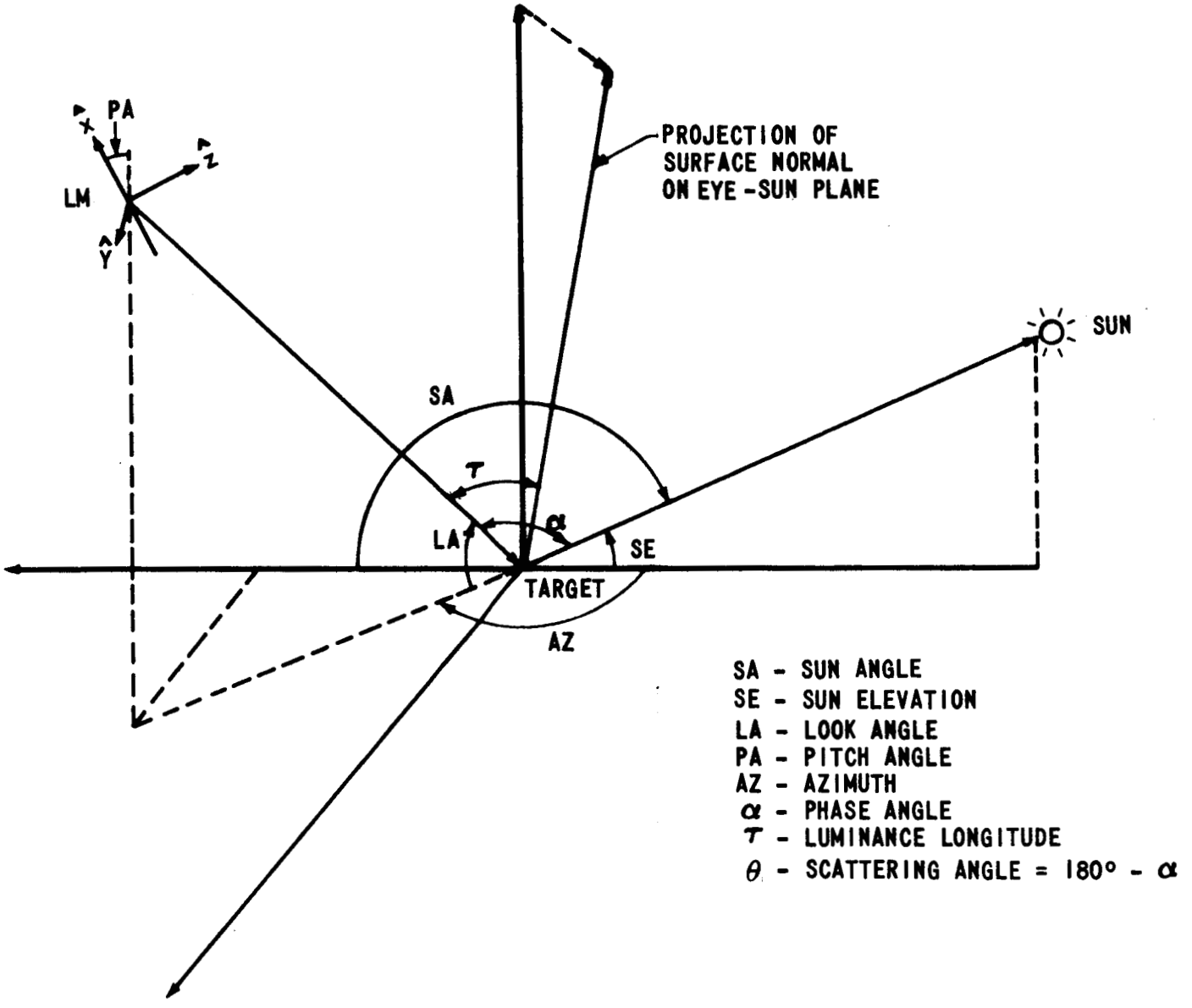

FIGURE 5 - DEFINITION OF ANGLES

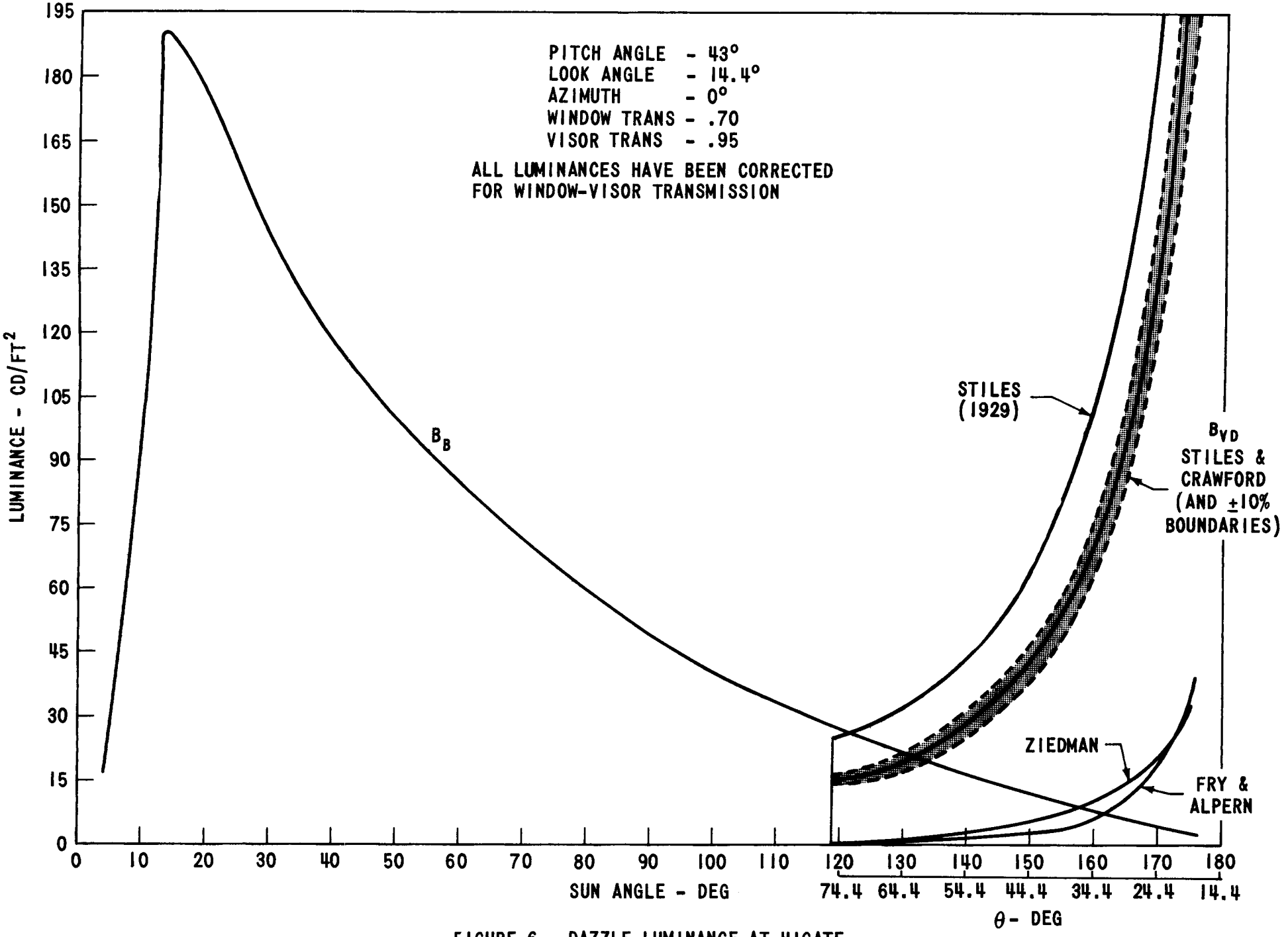

FIGURE 6 - DAZZLE LUMINANCE AT HIGATE

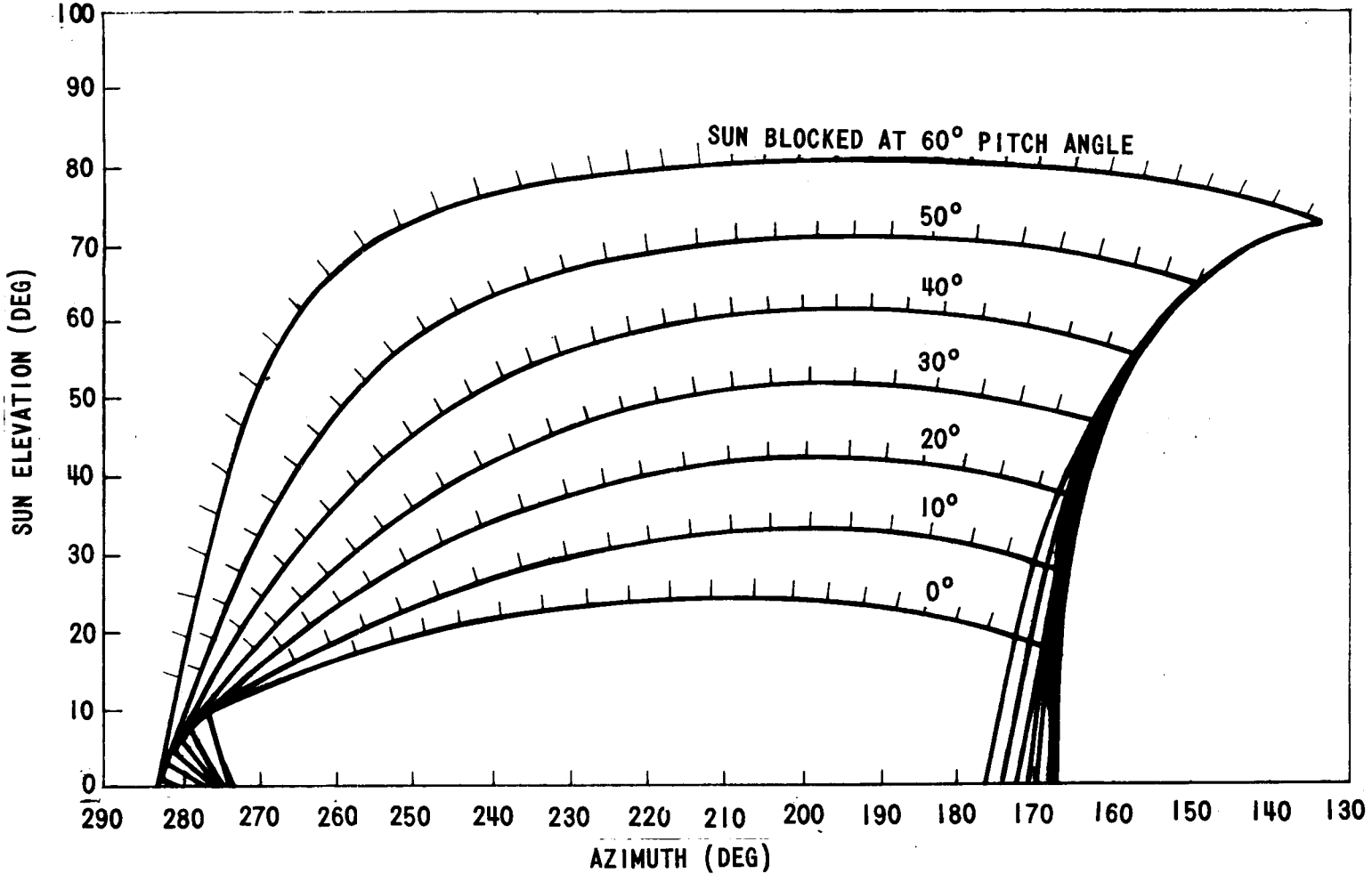

FIGURE 7 - SUN AND LM ANGLES FOR WHICH THE SUN IS IN THE COMMANDER'S EYE

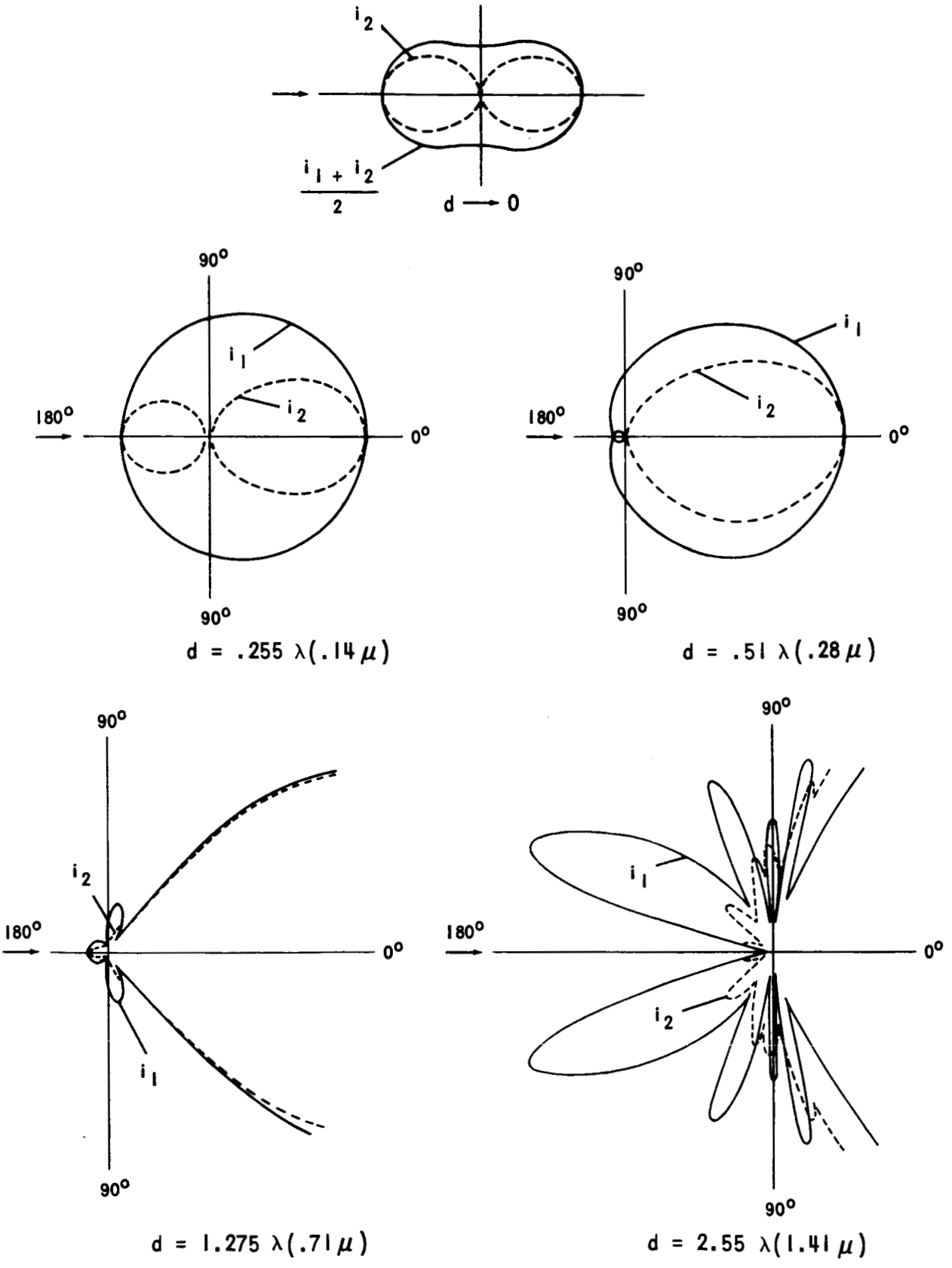

FIGURE 8 - POLAR DIAGRAMS OF THE SCATTER INTENSITY OF REPRESENTATIVE DIELECTRIC SPHERES OF PROGRESSIVELY LARGER DIAMETER FROM VERY SMALL TO ABOUT 2.5 WAVELENGTHS. IN THE LAST FOUR DIAGRAMS THE INTENSITIES OF THE TWO DIRECTIONS OF POLARIZATION, i_1 AND i_2, ARE SHOWN SEPERATELY. THEIR AVERAGE CORRESPONDS TO THE I USED IN THE TEXT. THE LIGHT IS INCIDENT FROM THE LEFT. FROM REFERENCE 28

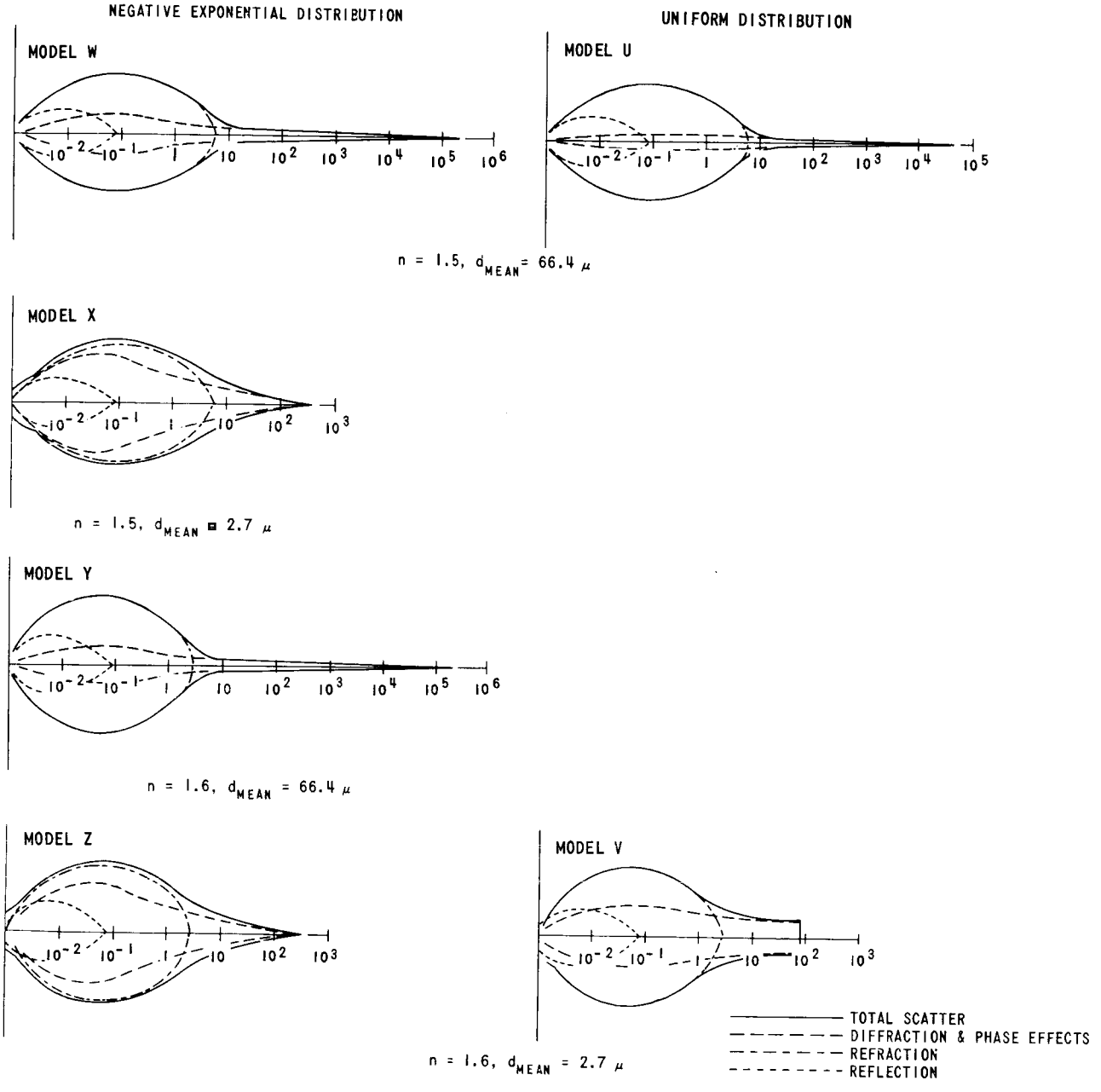

FIGURE 9 - POLAR PLOTS OF SCATTER INTENSITY/INCIDENT FLUX FOR MODELS USED IN THIS STUDY. THE LIGHT IS INCIDENT FROM THE LEFT.

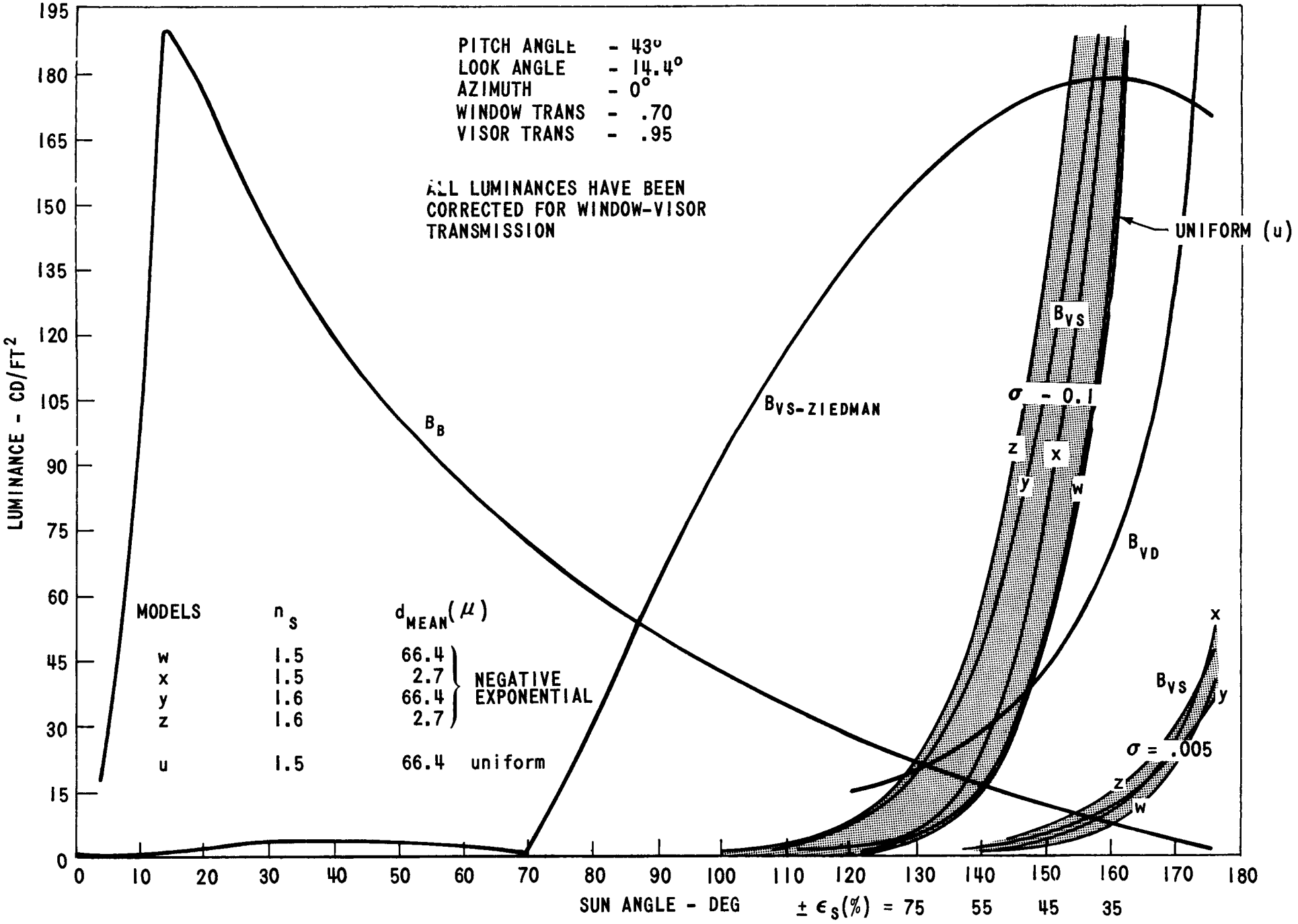

FIGURE 10 - SCATTER LUMINANCE AT HIGATE SHOWING VARIOUS SCATTER MODELS

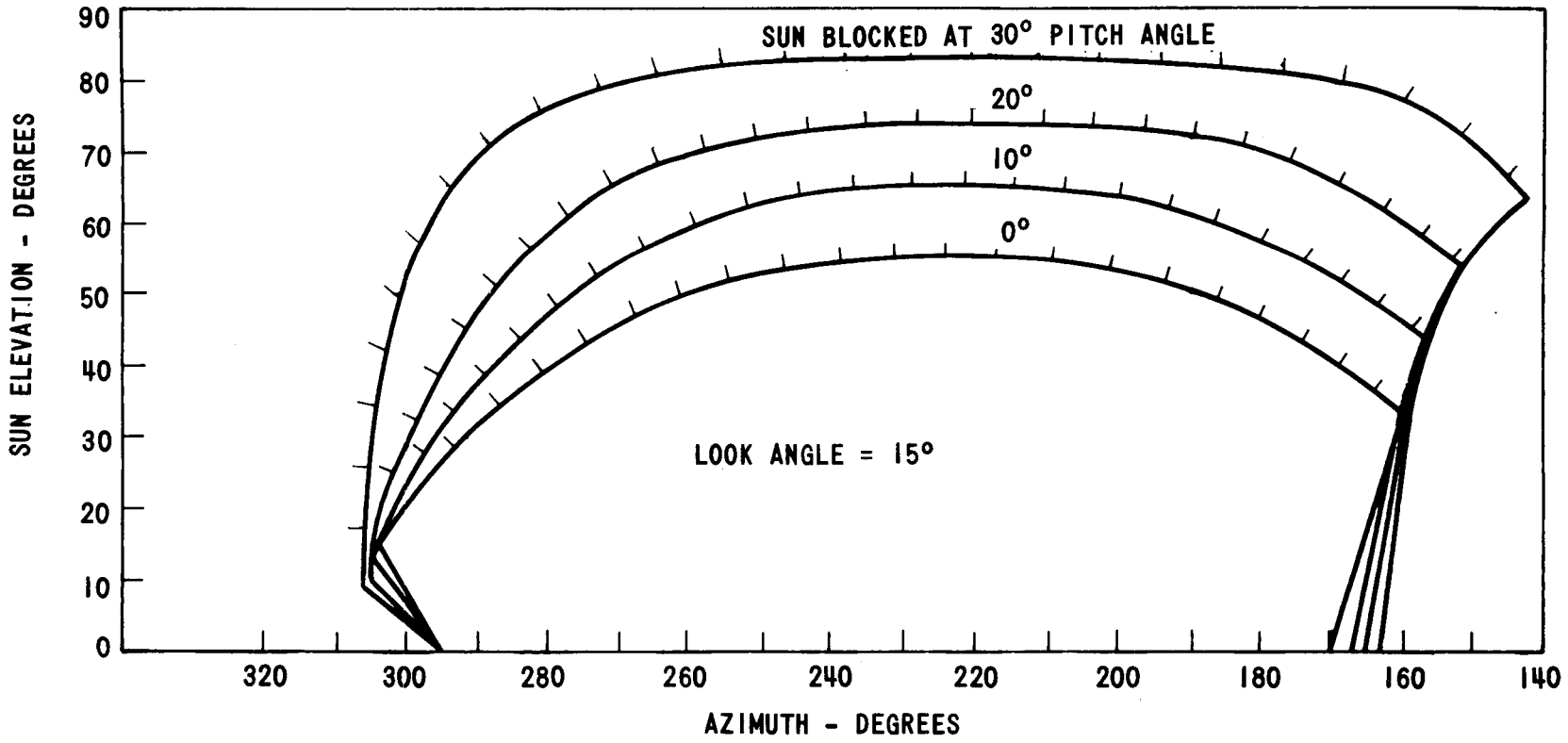

FIGURE 11 - ANGLES FOR WHICH THE SUN SHINES ON THE ACTIVE SCATTERING AREA DURING LUNAR DESCENT

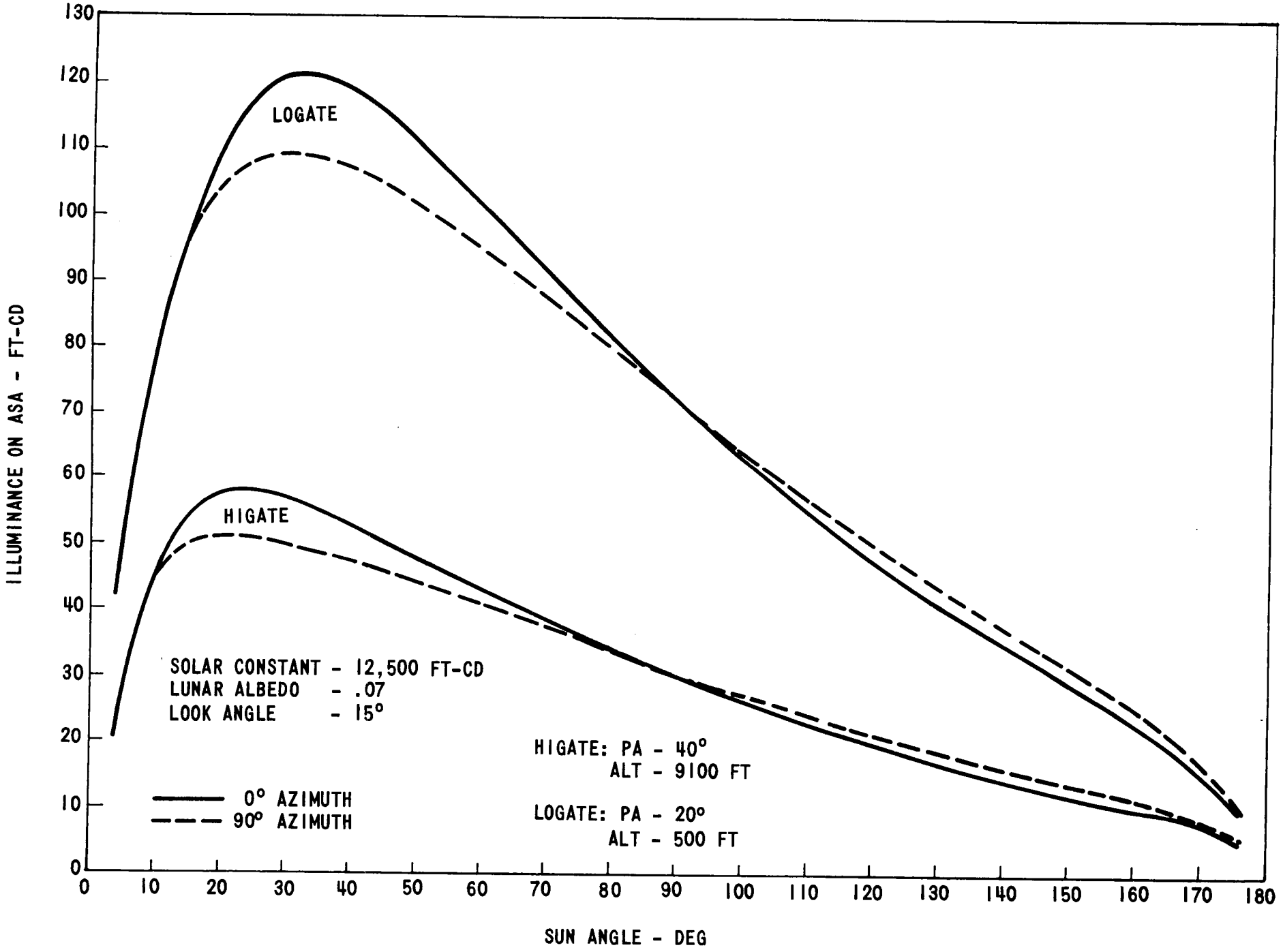

FIGURE 12 - ILLUMINANCE ON ASA DUE TO SUNLIGHT REFLECTED FROM THE LUNAR SURFACE

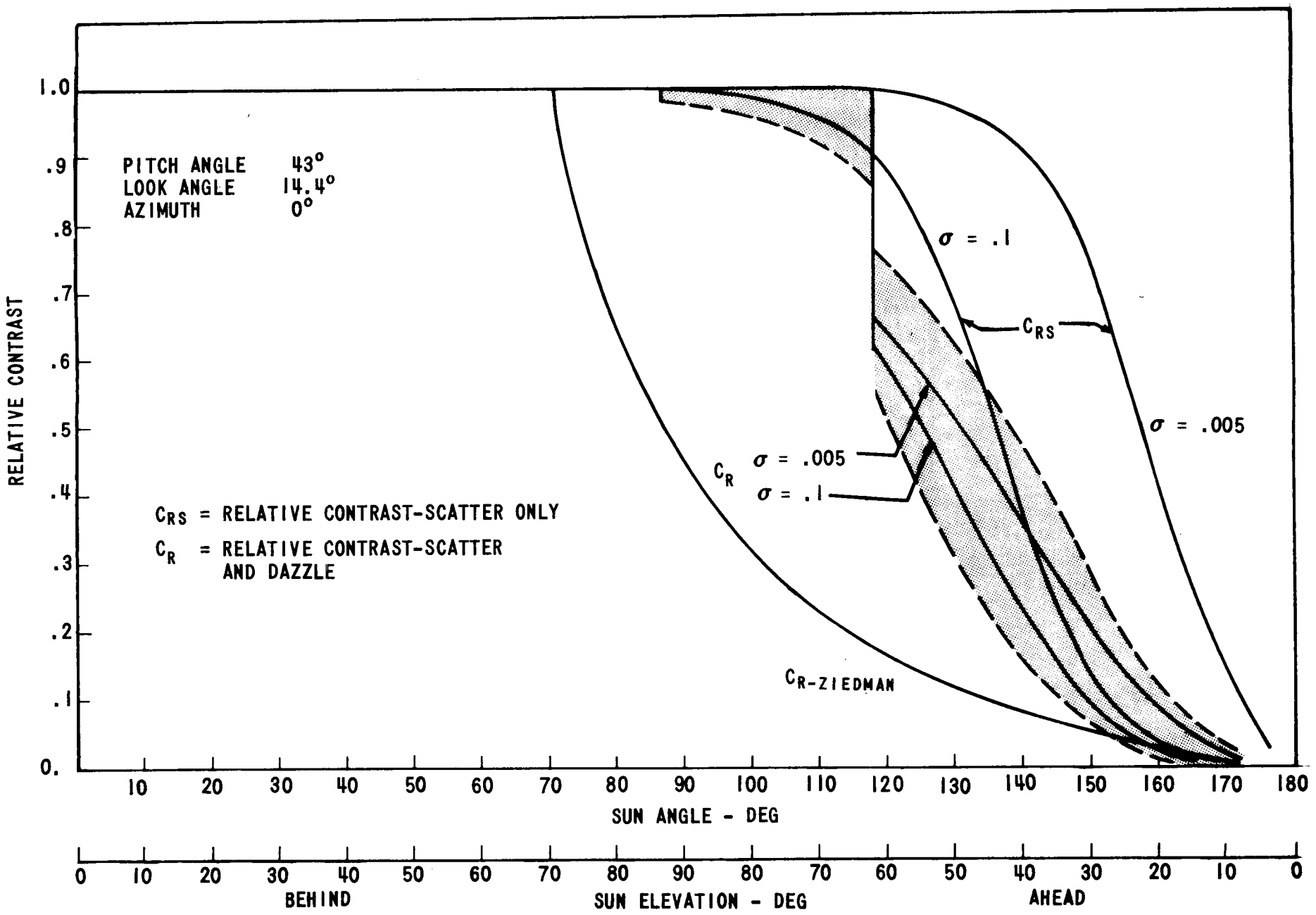

FIGURE 13 - RELATIVE CONTRAST AT HIGATE SHOWING ESTIMATED UNCERTAINTIES IN C_R

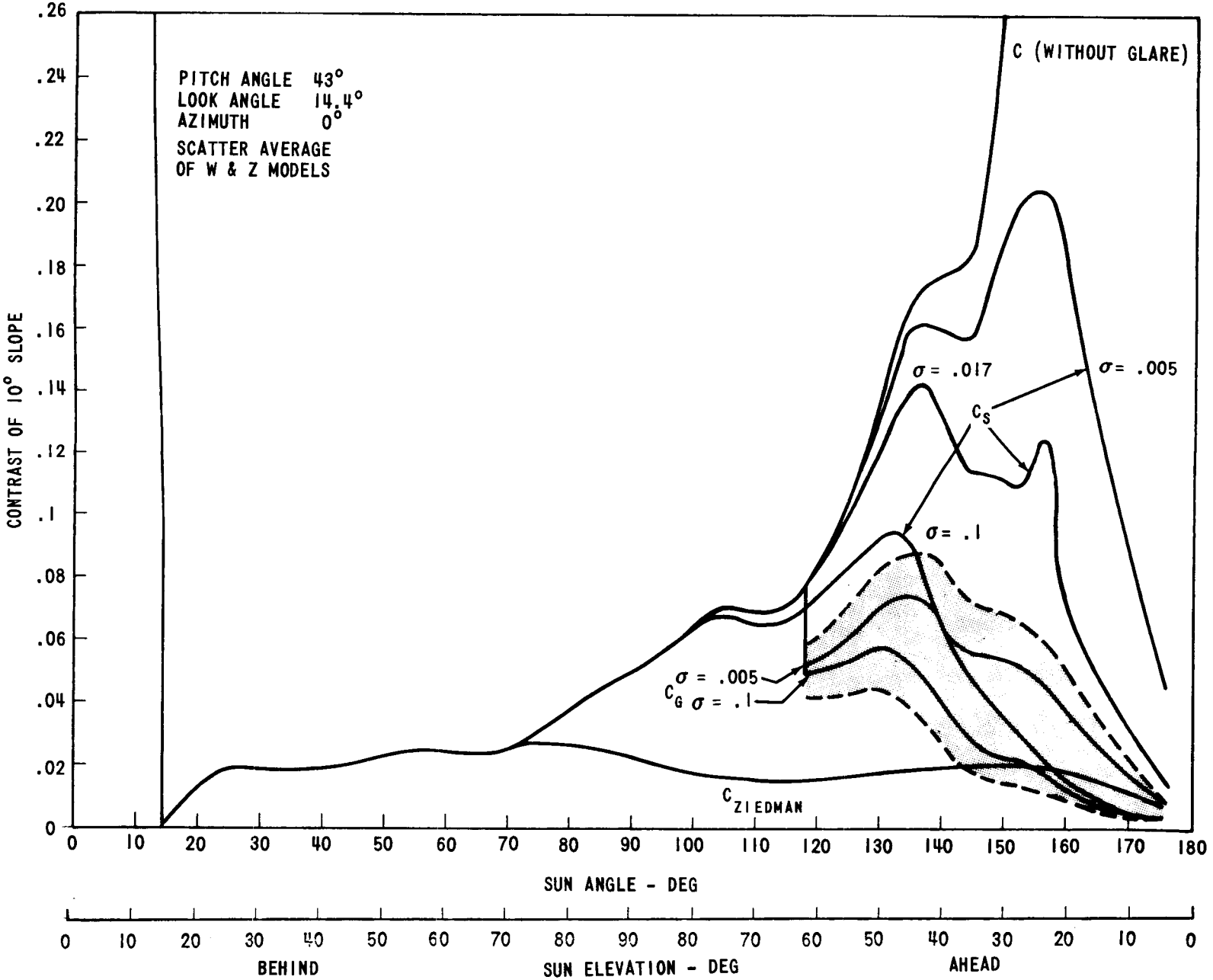

FIGURE 14 - CONTRAST WITH GLARE (C_G) AND CONTRAST WITH SCATTER ALONE (C_S) AT HIGATE SHOWING MINIMUM ESTIMATED UNCERTAINTIES IN C_G

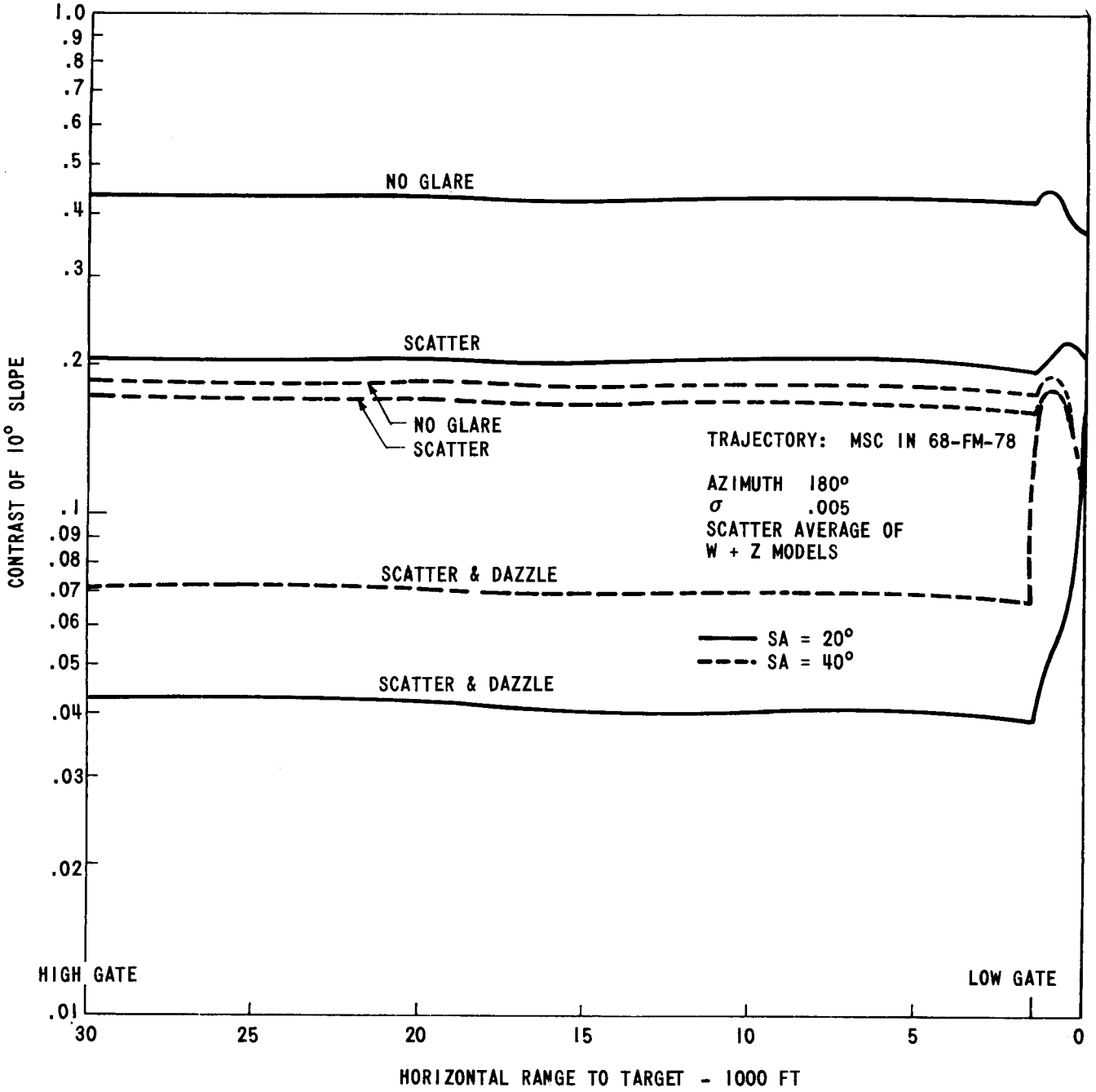

FIGURE 15 - SCENE CONTRAST DURING LM DESCENT AGAINST THE SUN
LOW SCATTER LEVELS

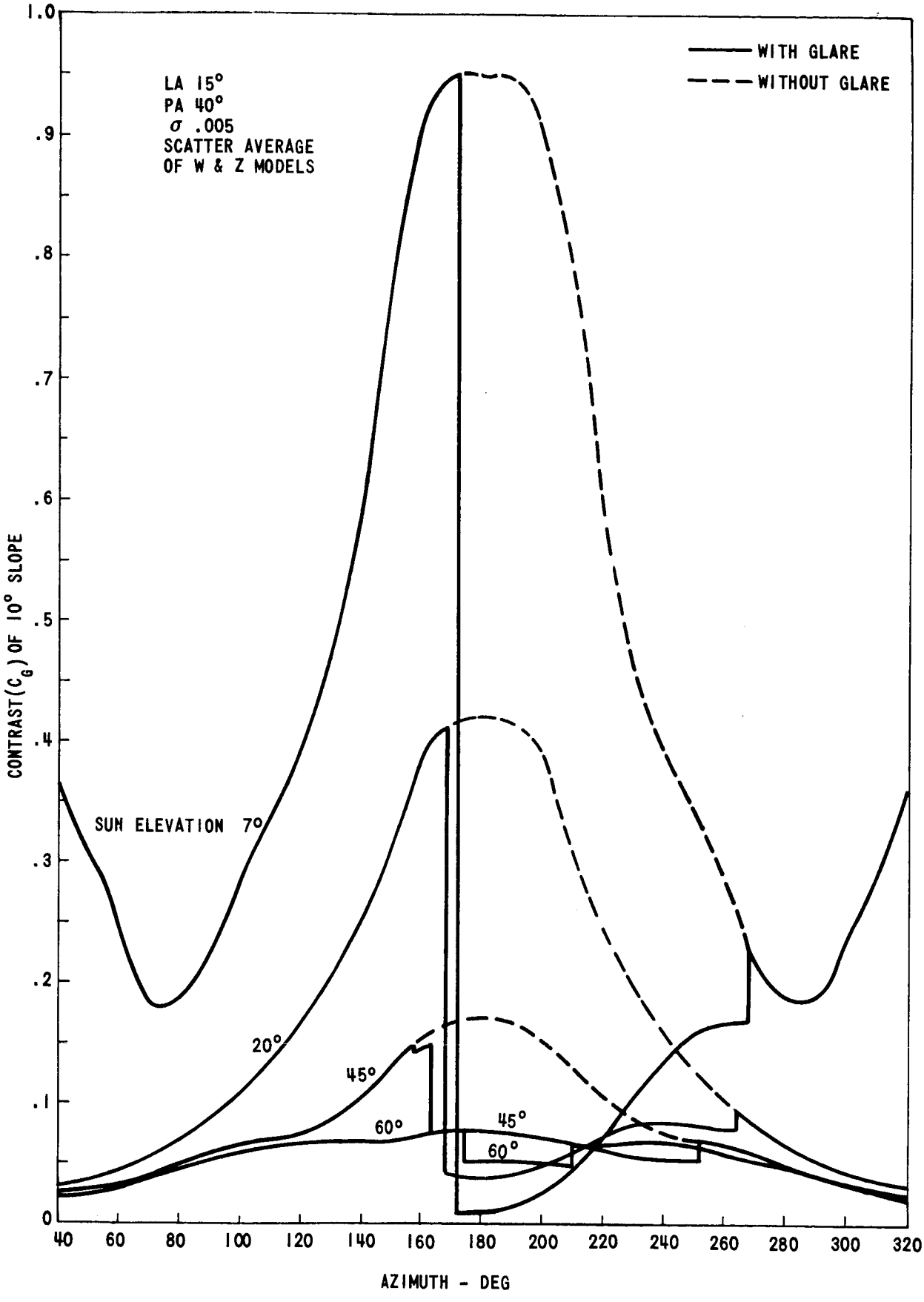

FIGURE 16 - CONTRAST AS A FUNCTION OF AZIMUTH INCLUDING SCATTER AND DAZZLE EFFECTS

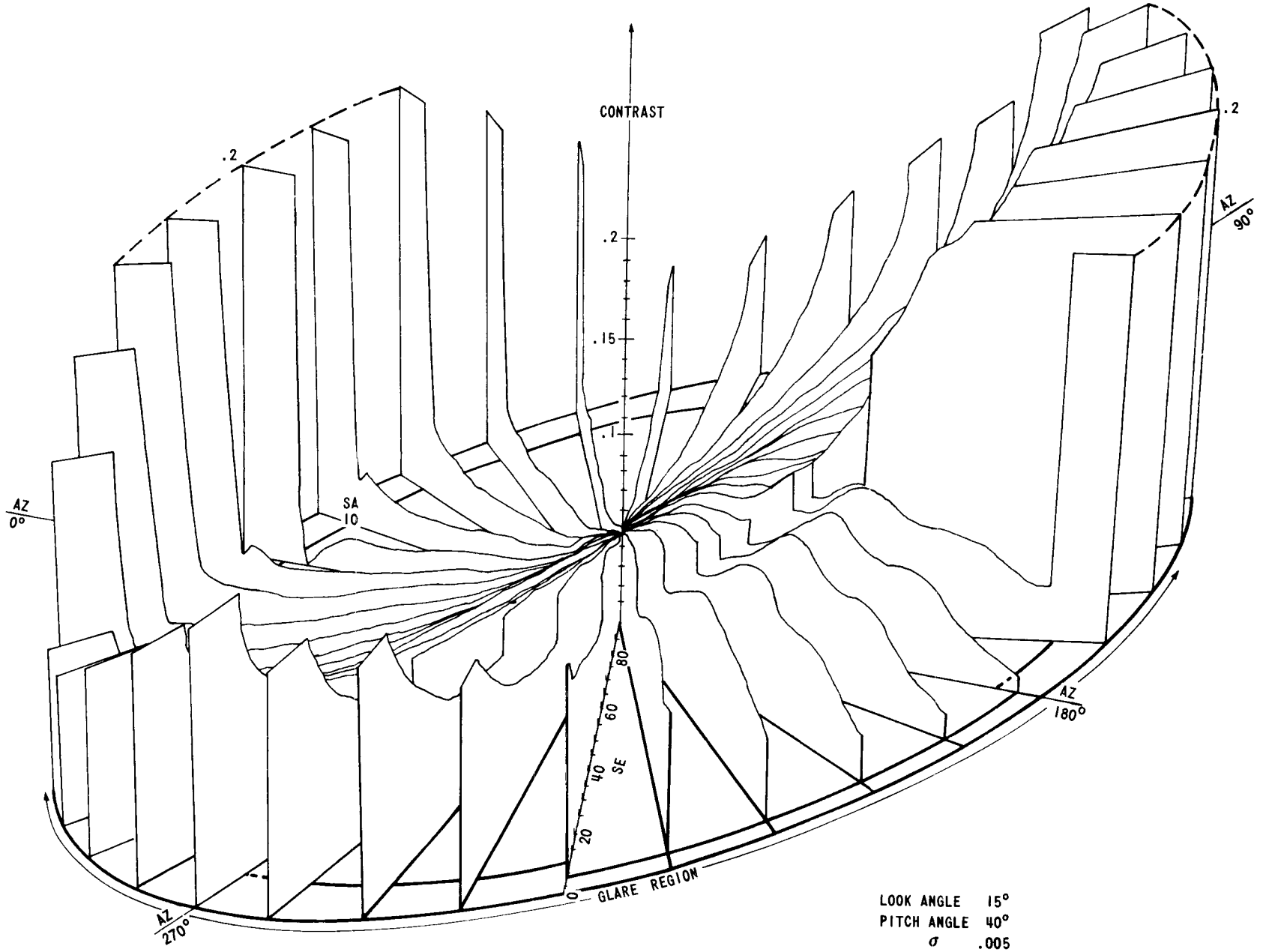

FIGURE 17a - CONTRAST OF A 10° SLOPE AS A FUNCTION OF SUN ELEVATION (SE) AND AZIMUTH (AZ) AT HIGATE - LOW SCATTER LEVEL

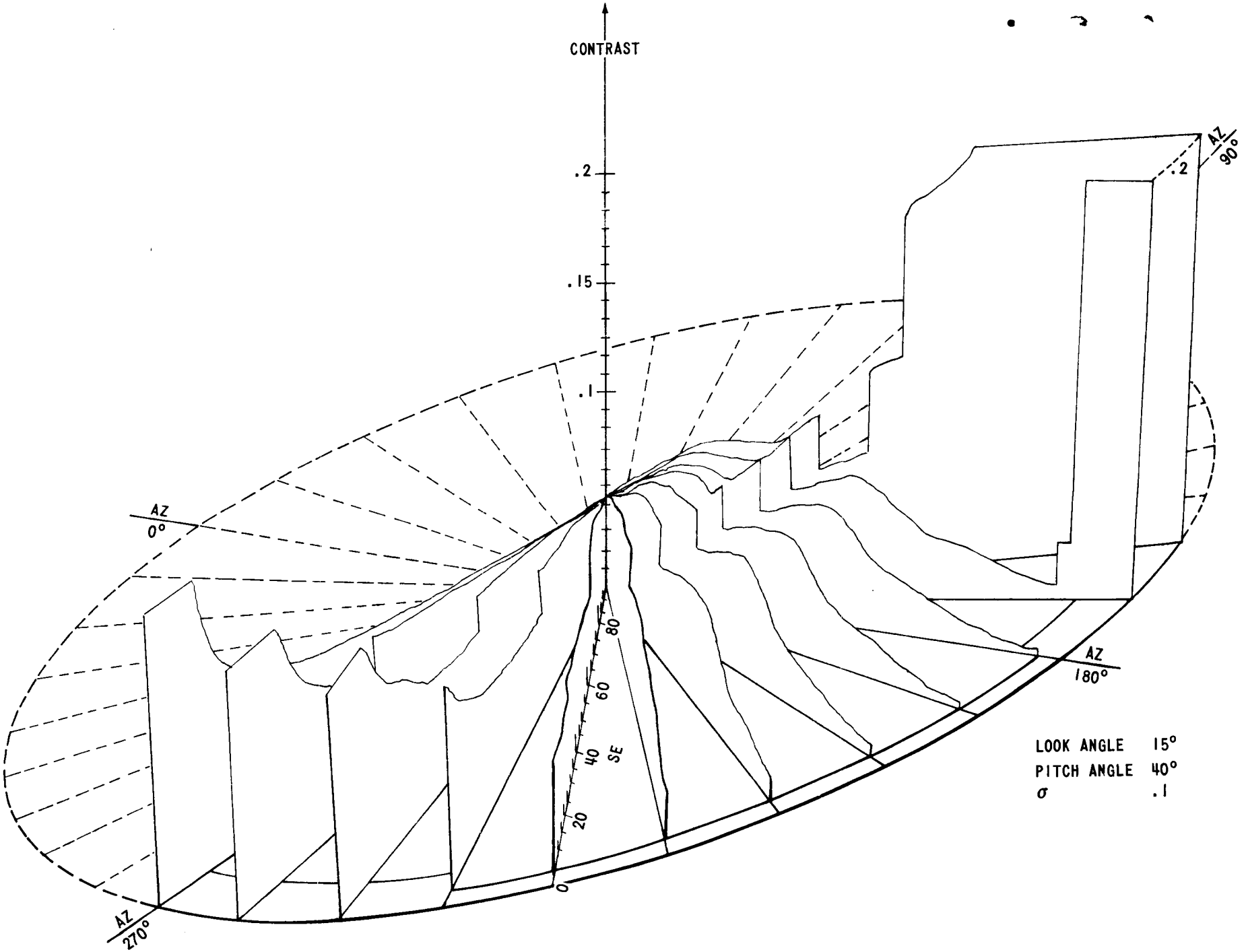

FIGURE 17b - CONTRAST OF A 10° SLOPE IN THE GLARE REGION AS A FUNCTION OF SUN ELEVATION (SE) AND AZIMUTH (AZ) AT HIGATE - HIGH SCATTER LEVEL

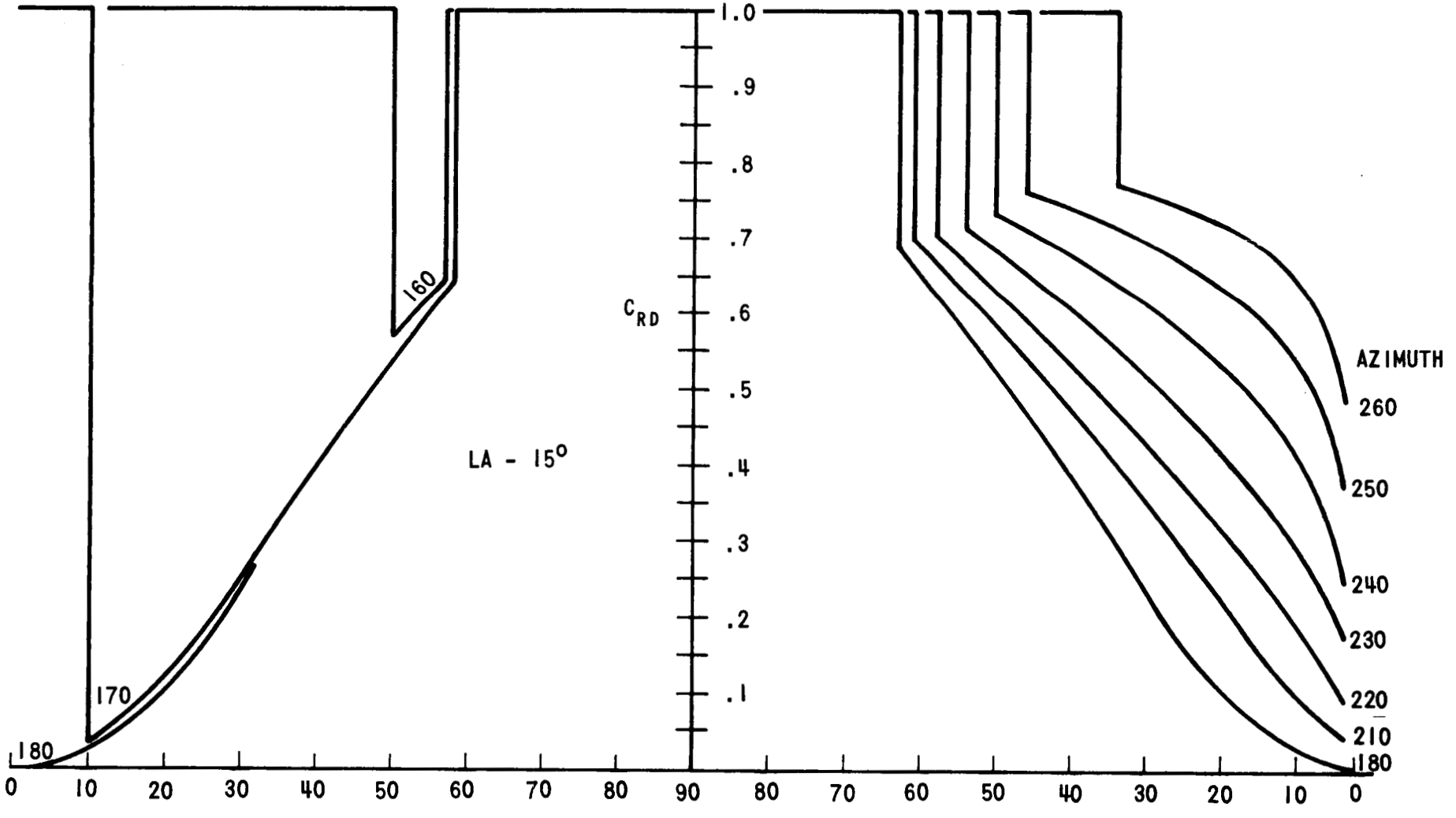

FIGURE 18 - C_{RD} AS A FUNCTION OF SUN ELEVATION

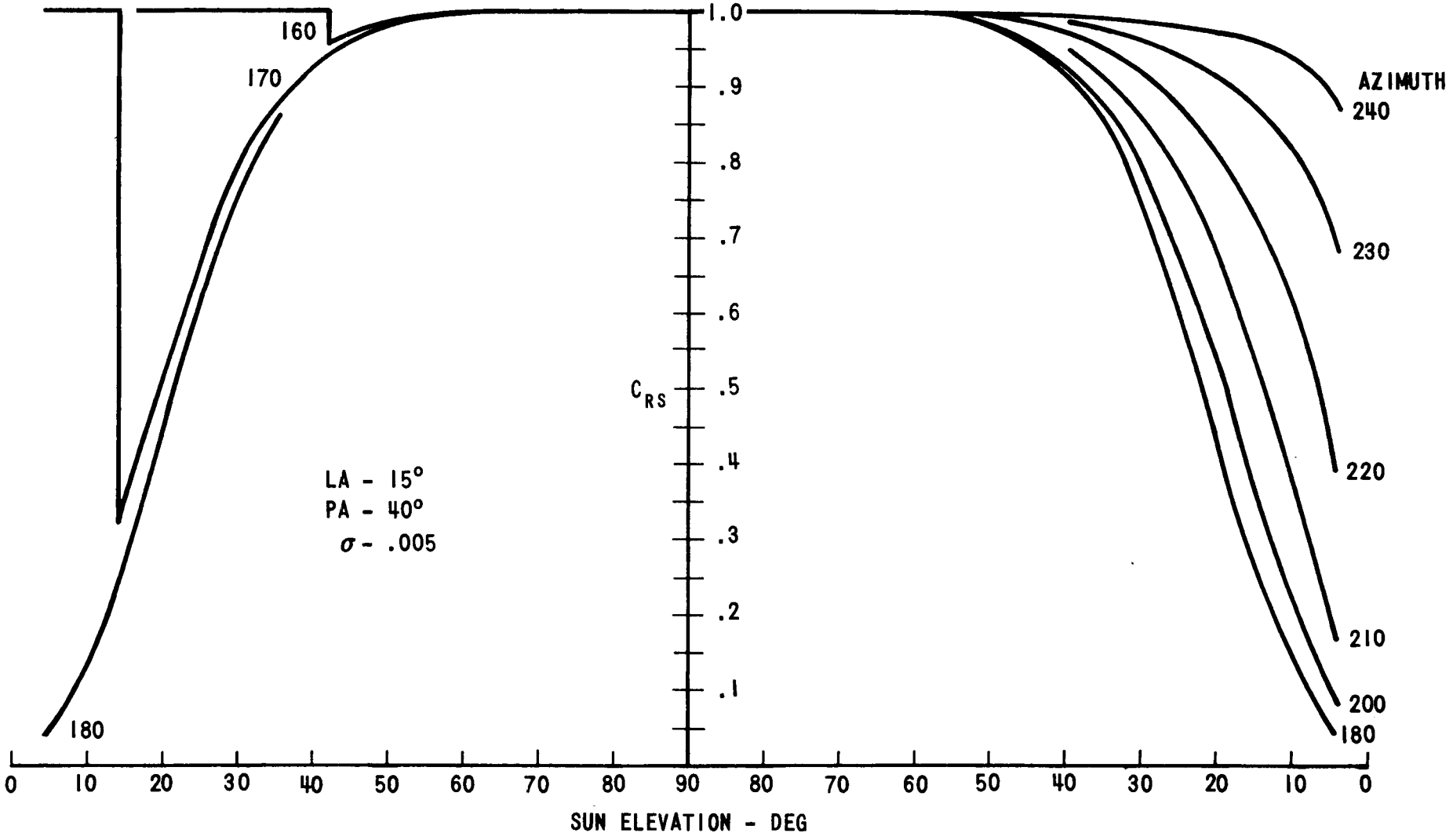

FIGURE 19 - C_{RS} AS A FUNCTION OF SUN ELEVATION AT LOW SCATTER LEVELS

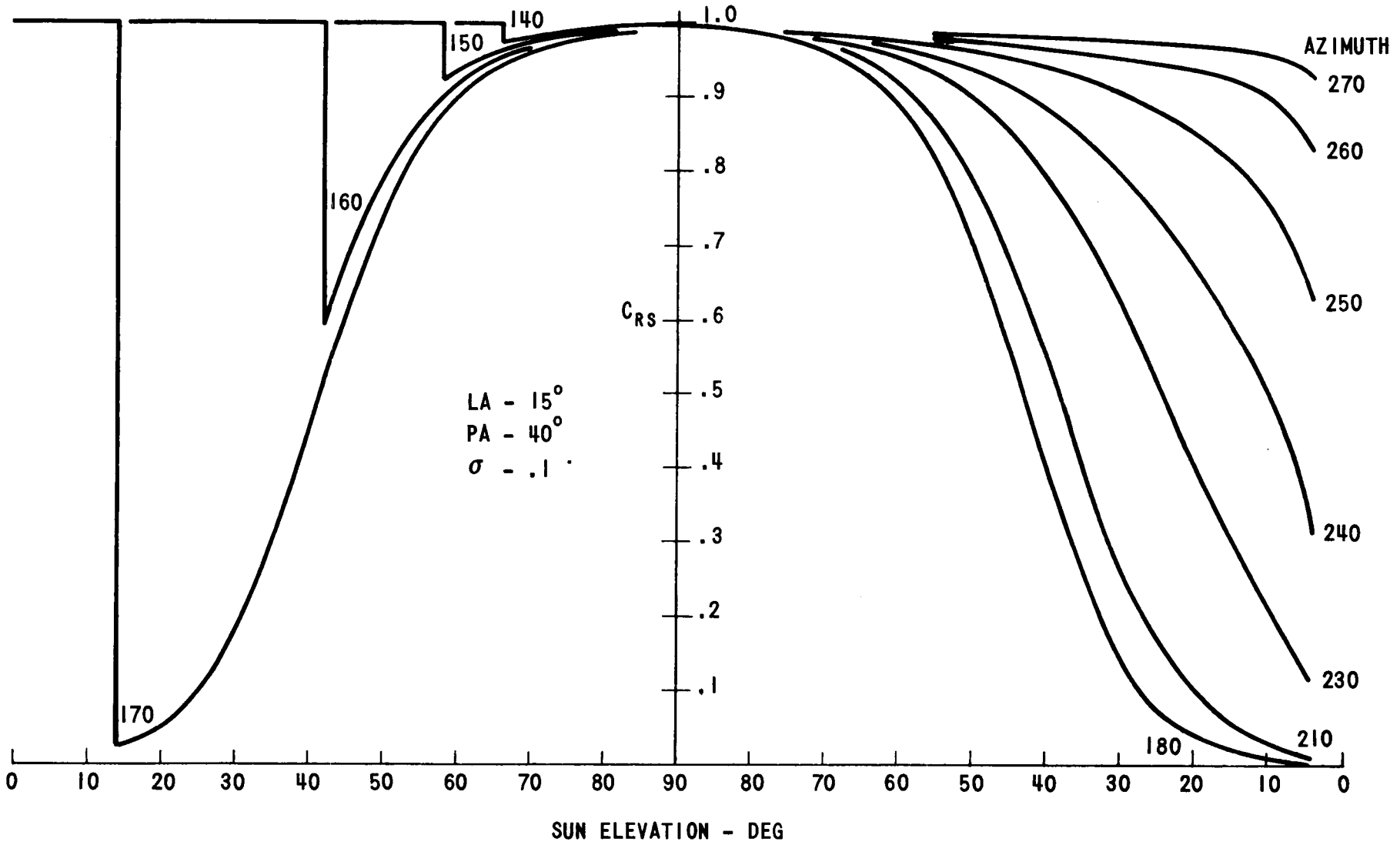

FIGURE 20 - C_{RS} AS A FUNCTION OF SUN ELEVATION AT HIGH SCATTER LEVELS